

Efficient count-based models improve power and robustness for large-scale single-cell eQTL mapping

Zixuan Eleanor Zhang^{1,**}, Artem Kim¹, Noah Suboc¹, Nicholas Mancuso^{1,2,3,**}, Steven Gazal^{1,2,3,**}

1. Center for Genetic Epidemiology, Department of Population and Public Health Sciences, Keck School of Medicine, University of Southern California
2. Department of Quantitative and Computational Biology, University of Southern California
3. Norris Comprehensive Cancer Center, Keck School of Medicine, University of Southern California

* contributed equally

** corresponding authors

Abstract

Population-scale single-cell transcriptomic technologies (scRNA-seq) enable characterizing variant effects on gene regulation at the cellular level (e.g., single-cell eQTLs; sc-eQTLs). However, existing sc-eQTL mapping approaches are either not designed for analyzing sparse counts in scRNA-seq data or can become intractable in extremely large datasets. Here, we propose jaxQTL, a flexible and efficient sc-eQTL mapping framework using highly efficient count-based models given pseudobulk data. Using extensive simulations, we demonstrated that jaxQTL with a negative binomial model outperformed other models in identifying sc-eQTLs, while maintaining a calibrated type I error. We applied jaxQTL across 14 cell types of OneK1K scRNA-seq data ($N=982$), and identified 11-16% more eGenes compared with existing approaches, primarily driven by jaxQTL ability to identify lowly expressed eGenes. We observed that fine-mapped sc-eQTLs were further from transcription starting site (TSS) than fine-mapped eQTLs identified in all cells (bulk-eQTLs; $P=1 \times 10^{-4}$) and more enriched in cell-type-specific enhancers ($P=3 \times 10^{-10}$), suggesting that sc-eQTLs improve our ability to identify distal eQTLs that are missed in bulk tissues. Overall, the genetic effect of fine-mapped sc-eQTLs were largely shared across cell types, with cell-type-specificity increasing with distance to TSS. Lastly, we observed that sc-eQTLs explain more SNP-heritability (h^2) than bulk-eQTLs ($9.90 \pm 0.88\%$ vs. $6.10 \pm 0.76\%$ when meta-analyzed across 16 blood and immune-related traits), improving but not closing the missing link between GWAS and eQTLs. As an example, we highlight that sc-eQTLs in T cells (unlike bulk-eQTLs) can successfully nominate *IL6ST* as a candidate gene for rheumatoid arthritis. Overall, jaxQTL provides an efficient and powerful approach using count-based models to identify missing disease-associated eQTLs.

35 Introduction

36 Large gene expression quantitative trait loci (eQTLs) studies have facilitated interpreting genetic variants
37 identified in genome-wide association studies (GWAS) through colocalization¹⁻⁴ or transcriptome-wide
38 association studies (TWAS)⁵⁻⁹. These approaches have been largely dependent on eQTLs discovered
39 from bulk-RNA sequencing (bulk-eQTLs) on tissue samples^{10,11} or on a limited number of cell types<sup>12-
40 14</sup>. However, limited overlap between bulk-eQTLs and GWAS risk loci^{4,10,15-18} has hindered the functional
41 interpretation of genetic risk variants and their translation to therapeutic development for human
42 diseases. Multiple hypotheses could explain this “missing link” between GWAS and eQTLs, including the
43 lack of disease-relevant cell types/contexts, cell-type-specific eQTL effects diluted in bulk samples, and
44 limited statistical power to detect weak-effect eQTLs^{15,16}.

45 Recent and ongoing generation of large scale single-cell RNA sequencing (scRNA-seq) datasets
46 allow direct interrogation of these hypotheses by quantifying gene expression across heterogeneous cell
47 types for a large number of individuals^{19,20}. For example, the OneK1K project has released scRNA-seq
48 data from 1.27 million peripheral blood mononuclear cells (PMBCs) of 982 donors¹⁹, with plans to profile
49 50 million cells in 10,000 donors (TenK10K)²¹. A current challenge is thus to efficiently identify single-
50 cell (sc-)eQTLs from sparse counts data in these extremely large datasets. Previous sc-eQTL studies<sup>22-
51 26</sup> have leveraged pseudobulk data and used tools that are designed for bulk-eQTL mapping (e.g., Matrix
52 eQTL²⁷, FastQTL²⁸, and tensorQTL²⁹). These tools fit linear models after data normalization on the
53 gene expression matrix^{30,31}. Although the model fitting step is computationally efficient, the eQTL effect
54 on gene expression is less interpretable due to the data transformation (e.g., inverse rank transform).
55 Moreover, for sparse read counts observed in scRNA-seq, transformations are less effective due to sheer
56 number of zeros^{32,33}. Recent studies have proposed modelling the expression of single cells by fitting
57 mixed effect models, either using off-the-shelf R functions³⁴ or under bespoke software such as
58 CellRegMap³⁵ and SAIGE-QTL³⁶. While these approaches improve upon bulk-eQTL mapping
59 approaches, they can become computationally intractable for extremely large single-cell datasets
60 currently being generated at a population scale. In addition to these computational challenges, the
61 characterization of sc-eQTLs across cell types is further complicated by the differential statistical power
62 induced by differences in cell abundances. For example, recent work reported sc-eQTLs were largely
63 cell-type-specific¹⁹, in contrast to higher levels of sharing across cell types when eQTLs were identified
64 from sorted RNA-seq data³⁷. Therefore, sc-eQTL mapping and characterization stands to benefit from
65 scalable and statistically powerful software.

66 To address these limitations, we propose jaxQTL, an efficient software to perform large-scale sc-
67 eQTL mapping using flexible, count-based models. Under simulations, we found that a negative binomial
68 (negbinom) model outperforms linear and Poisson models in identifying sc-eQTLs while maintaining
69 calibrated type I errors. By analyzing OneK1K, we found that jaxQTL with a negative binomial model
70 identifies more eGenes than other models and existing softwares, such as tensorQTL and SAIGE-QTL.
71 Importantly, we found that sc-eQTLs effects were largely consistent across cell types, with cell-type-
72 specificity increasing with distance to transcription start site. Finally, we found that sc-eQTLs explained
73 a greater fraction of heritability for GWAS immune traits compared with bulk-eQTLs, thus improving but
74 not closing the missing link between GWAS and eQTLs. Taken together, our results demonstrate that
75 jaxQTL is a scalable tool in identifying sc-eQTLs by analyzing large single-cell datasets to improve the
76 biological interpretation of genetic risk at disease-relevant cell types.

77 Results

78 Overview of jaxQTL

79 We provide a brief overview of jaxQTL model assumptions and inferential pipeline. Given pseudobulk
80 counts y_c for a focal gene in a cellular context c (i.e. summed across all cells of type c), covariates X
81 (e.g., age, sex, genotyping principal components), and a cis-genetic variant g , jaxQTL implements a
82 generalized linear model (GLM) according to,

$$83 \quad E[y_c | X] = h(X\beta + g\beta_g + l_c),$$

84 where β are the covariate effects, β_g is the allelic effect, l_c is an offset adjusting for differences in library
85 size, and $h(\cdot)$ is a function which maps linear predictions to expected values matching distribution
86 assumptions (e.g., negbinom, Poisson). For example, if we assume a Poisson or negative binomial
87 distribution, then $h := \exp(\cdot)$, with effect sizes reflecting a change in the transcription rate (or proportion
88 if including library size offsets). This is in contrast to linear regression performed on the rank-inverse
89 normal transformed counts, where effect sizes have no direct interpretation of the expression values, but
90 rather reflect a change in rankings.

91 Performing cis-association scans using this approach is computationally prohibitive, due to the
92 sheer number tests required for each gene and cell-type. To address this fundamental limitation, jaxQTL
93 leverages three key insights. First, jaxQTL performs *just-in-time* (JIT) compilation provided by the JAX
94 framework (**Web Resources**), to translate high-level Python into machine-level instructions optimized for
95 a specific parallelized architectures (e.g., CPU, GPU, or TPU) with no additional work required from the
96 user other than a runtime flag. Second, jaxQTL performs a score-test³⁸ for all cis-genetic variants
97 simultaneously using an optimized block-matrix approach, rather than sequentially. Lastly, jaxQTL
98 implements multiple recent advances to compute p-values efficiently, which provide trade-offs between
99 additional scalability and statistical power (e.g., Beta-approximation²⁸ to permutations or ACAT-V³⁹;
100 **Figures S1, S2; Methods**). We provide a table summarizing the capabilities of jaxQTL alongside other
101 softwares (**Table S1**) and have released jaxQTL as open-source software (see **Code availability**).

102 Negative binomial outperforms other models in identifying sc-eQTLs in 103 realistic simulations

104 We assessed the type I error and power of different models implemented in jaxQTL (jaxQTL-linear,
105 jaxQTL-negbinom, and jaxQTL-Poisson) and softwares (SAIGE-QTL and tensorQTL) by simulating
106 single-cell read counts from a Poisson mixed effect (PME) generative model using parameters that reflect
107 observed expression and overdispersion in OneK1K^{30,40–46} (**Figure S3, S4**). We evaluated model
108 performance across varying cell type proportions by sampling individual library sizes across three cell
109 types representing high, medium, and low library sizes (CD4+ naïve and central memory T (CD4_{NC}) cells,
110 immature and naïve B (B_{IN}) cells, and Plasma cells, respectively; **Table S2**). We varied sample-coverage
111 (i.e., the percentage of non-zero expression read counts) across simulations to account for gene
112 expression intensity across individuals.

113 First, all models exhibited calibrated type I error rates when simulating from the single-cell PME
114 model (**Figure 1A**), except for pseudobulk jaxQTL-Poisson which displayed increased false positives
115 likely due to its over-conservative standard errors. We observed largely similar conclusions for jaxQTL
116 when varying heritability, random intercept variance σ^2_u (modeling similarity of cell read counts within
117 the same person; see **Methods**), sample size, and minor allele frequency (MAF) parameters (**Figures**
118 **S5-S8**). Importantly, jaxQTL-negbinom and linear models remain calibrated across cell type abundances
119 and sample sizes, unlike SAIGE-QTL which exhibited increased false positives in rarer cell types when
120 sample sizes are small ($N < 200$; **Figure S7**). SAIGE-QTL and jaxQTL-negbinom had slight inflation when
121 $\sigma^2_u \approx 1$, however this scenario is unlikely to occur in practice (**Figure S3**).

122 Next, we observed that jaxQTL-negbinom had improved power compared with jaxQTL-linear and
123 tensorQTL, especially for lower coverage genes. Across three cell types, genes with higher coverage
124 exhibited greater statistical power to identify their sc-eQTLs. Specifically, for large cell type proportions,
125 jaxQTL-negbinom outperformed jaxQTL-linear for genes with $>95\%$ coverage ($P = 7.53 \times 10^{-4}$). For
126 medium and rare cell types, jaxQTL-negbinom exhibited greater power over jaxQTL-linear down to $\sim 70\%$
127 coverage ($P = 2.02 \times 10^{-4}$ and 3.91×10^{-27} respectively), highlighting the benefit of count-based models
128 for lower expressed genes and rarer cell types. While both jaxQTL-linear and tensorQTL fit linear models
129 of gene expression, differences in power can be explained by jaxQTL score test versus tensorQTL Wald
130 test. We obtained similar conclusions when varying heritability, random intercept variance σ^2_u , sample
131 size, and MAF parameters (**Figures S5-S8**).

132 After assessing model performances under the PME model with non-zero random intercept
133 variance σ^2_u , we repeated our analyses by sampling read counts from PME models with $\sigma^2_u = 0$, which
134 reflects a standard Poisson model (**Figure S9**). As expected, the performance of jaxQTL-negbinom and
135 SAIGE-QTL closely resembled jaxQTL-Poisson (see **Supplemental Note**). Again, count-based models
136 outperformed jaxQTL-linear and tensorQTL, notably for genes in rarer cell types. All models were well-
137 calibrated under the null.

138 Altogether, jaxQTL-negbinom provides a calibrated and powerful pseudobulk model for single-
139 cell data that performs comparably to the PME model of SAIGE-QTL. Our empirical results can be in part
140 explained by the structural similarity of the variance under negative binomial and PME models of
141 pseudobulk (see **Supplemental Note**).

142 jaxQTL improves power for eGene discovery in the OneK1K dataset

143 To benchmark jaxQTL in identifying eGenes on real datasets, we applied jaxQTL on single-cell data of
144 14 PBMC cell types from $N = 982$ individuals in OneK1K¹⁹. We defined eGene as genes with at least
145 one sc-eQTL in a cell type, i.e., gene-cell-type pairs. Before comparing different sc-eQTL models, we
146 investigated the calibration of gene-level P values obtained by the Beta-approximation approach that
147 permutes the gene expressions observed in OneK1K data. Across the three representative cell types,
148 we found that gene-level P values from jaxQTL-linear and jaxQTL-negbinom were well-calibrated (**Figure**
149 **S10**), however gene-level P values for jaxQTL-Poisson were inflated due to overcorrection by the
150 permutation method on its variant P values.

151 After confirming the gene-level P values were calibrated, we compared the statistical power in
152 identifying eGenes across different models using jaxQTL (**Figure 2A**; **Table S3**). Across 14 cell types,

153 jaxQTL-negbinom identified 14% more eGenes compared with jaxQTL-linear (18,907 vs. 16,654 eGenes,
154 $P = 1 \times 10^{-35}$), and 21% more compared with jaxQTL-Poisson (15,634 eGenes, $P = 5 \times 10^{-75}$). The number
155 of eGenes found per cell type was highly correlated with cell type proportions, which reflects differential
156 statistical power (Pearson $\rho = 0.97$; **Figure S11**). Focusing on jaxQTL-negbinom and jaxQTL-linear, we
157 found the negbinom model provided higher χ^2 test statistics for lead SNP-eGene pairs across cell types
158 (median $\chi^2 = 43.60$ vs. 38.46, $P = 3 \times 10^{-24}$; **Figure S12**). eGenes identified between models show
159 substantial overlap (**Figure S13A**). Consistent with simulation results, eGenes identified exclusively by
160 jaxQTL-negbinom had lower coverage (median 79% vs. 94%, $P = 2 \times 10^{-115}$; **Figure S13B**) than eGenes
161 also identified with jaxQTL-linear, confirming that the negbinom model is more powerful for genes with
162 lower expression. The reduced power of the jaxQTL-Poisson was caused by the penalty on its inflated
163 type I error when computing the gene-level P values using the permutation approach. Given the
164 improvement of the negbinom model over Poisson and linear models, to simplify our presentation we
165 refer to jaxQTL-negbinom as jaxQTL for the remainder of the manuscript.

166 We next compared jaxQTL performance against tensorQTL²⁹ (a commonly used software for
167 bulk-eQTL mapping using a linear model) and SAIGE-QTL³⁶ (a recent software for sc-eQTL mapping
168 using a Poisson mixed-effect model) (**Figure 2B**; **Table S4**). Across 14 cell types, jaxQTL identified 16%
169 more eGenes compared with tensorQTL ($P = 2 \times 10^{-47}$) and 11% more eGenes compared with SAIGE-
170 QTL ($P = 3 \times 10^{-24}$), thus demonstrating jaxQTL increased power to identify eGenes in both rare and
171 common cell types. The advantage of jaxQTL over SAIGE-QTL can be partially explained by gene-level
172 calibration methods (permutation vs. ACAT-V), as performance gap decreased when applying ACAT-V
173 in jaxQTL (5% more eGenes; **Figure 2B**). We note that our tensorQTL results identified more eGenes
174 than tensorQTL in ref.³⁶, likely due to different procedures to create pseudobulk data (see **Methods**).
175 Finally, we confirmed that jaxQTL-linear results agreed with our tensorQTL results since the Wald test
176 and score test are asymptotically equivalent (97% overlap; **Figure S14**), with differences up to gene-level
177 P value obtained by the permutation approach.

178 Next, we evaluated the computational performance of jaxQTL in cis-eQTL mapping compared
179 with existing approaches using 50 randomly selected genes from chromosome 1 in OneK1K (see
180 **Methods**; **Figure S15**). The average run time of jaxQTL on GPU/TPU across 3 cell types is 3.7x faster
181 compared with SAIGE-QTL (12 vs. 44 mins) and 9.2x slower compared with tensorQTL (1.3 mins). To
182 demonstrate the impact of sample size on run time, we simulated data for varying sample size by
183 downsampling from $N=100$ to 700. The average run time is 39 mins for SAIGE-QTL, 15 mins for jaxQTL
184 on GPU/TPU, and 2 mins for tensorQTL. To mimic TenK10K data²¹, we performed upsampling to
185 simulate data for $N=10,000$ (see **Methods**). Focusing on a dominant cell type such as CD4_{NC} cells,
186 jaxQTL on GPU was at least 1,560x faster (30 mins) compared with SAIGE-QTL, highlighting the
187 efficiency of jaxQTL when applied to ever-increasing population-scale single-cell data. We note that the
188 runtime of jaxQTL is dominated by performing permutations. Importantly, when performing ACAT-V to
189 compute gene-level P values on CPU, jaxQTL was 1.3 - 10,596x times faster than SAIGE-QTL for $N=100$
190 to 10,000, and comparable with the linear model of tensorQTL (with permutations).

191 In summary, jaxQTL outperforms other models and methods in identifying eGenes in OneK1K,
192 highlighting that pseudobulk-approaches for scRNA-seq are powerful (even for rarer cell types) when
193 appropriately modeling count data. In addition, we observed that its computation time can scale to
194 scRNA-seq datasets with thousands of individuals approaching that of classical linear models.

195 jaxQTL results replicate across datasets and ancestries

196 To verify that increased eGene detection from jaxQTL is not driven by false positives, we first replicated
197 our sc-eQTLs results in 88 European- and 88 Asian-ancestry individuals from CLUES PBMC scRNA-seq
198 study (**Figure 3; Figure S16, S17; Table S5**)⁴⁷. Of the lead SNP-eGene pairs found in matched CLUES
199 cell types, 40-86% can be replicated in a European cohort and 23-74% in an Asian cohort at FDR < 0.05
200 with concordant directional effect. Additionally, we replicated 75-92% sc-eQTLs in EUR whole blood
201 samples from GTEx (N=588)¹⁰ and 50%-78% in FACS-sorted immune cell types from DICE study
202 (N=91)⁴⁸ (**Figure S18; Table S6**). We also observed consistent direction of sc-eQTL effects when
203 comparing with shared lead SNP-eGene results in original OneK1K results (**Figure S19**). Lastly, we
204 recapitulated the depletion of selection constraint and short enhancer domains in eGenes^{10,49,50} (**Figure**
205 **S20**; see **Web resources**). Consistent with refs.^{49,51-53}, we observed genes depleted of loss-of-function
206 mutations (pLI > 0.9) had smaller sc-eQTL effect sizes (**Figure S21**), and that the effect size of lead
207 SNPs of eGenes was smaller at lower allele frequency (**Figure S22**), confirming selection constraints on
208 gene expressions in immune cell types. Altogether, these results demonstrate that jaxQTL results
209 replicate across datasets and recapitulate known findings from bulk-eQTL studies.

210 sc-eQTLs are more enriched in cell-type-matched CREs than bulk- 211 eQTLs

212 To characterize sc-eQTLs and their potential downstream role in human diseases, we performed fine-
213 mapping for eGenes identified by jaxQTL on OneK1K using the SuSiE summary statistics approach⁵⁴.
214 Briefly, SuSiE performs Bayesian variable selection to identify likely causal SNPs in the form of credible
215 sets and provide posterior inclusion probabilities (PIPs) to quantify uncertainty in its selection (see
216 **Methods**). After restricting to the 18,281 non-MHC and non-MAPT eGenes identified by jaxQTL, SuSiE
217 reported 95% credible sets (CS) for 12,978 eGenes across 14 cell types (6,776 unique eGenes). The
218 average number of CSs per eGene was 1.15 with a median size of 16 SNPs, with 88% of eGenes
219 explained by a single causal variant. We observed that the average number of CSs tracked with cell type
220 proportion ($P = 1.49 \times 10^{-5}$; **Figure S23**), suggesting the fine-mapping results were likely biased by lower
221 statistical power to pinpoint independent causal eQTLs in rarer cell types. To establish a baseline, we
222 also performed cis-eQTL and fine-mapping analyses using “bulk” gene expression (i.e., summed over
223 cell types). As expected, we found that sc-eQTLs successfully identified a CS for more unique eGenes
224 than bulk-eQTLs (6,776 vs 6,338, $P = 9.5 \times 10^{-23}$).

225 To characterize the functional architecture of fine-mapped sc-eQTLs, we performed enrichment
226 analysis using cell-type-agnostic annotations from S-LDSC baseline model⁵⁵ (see **Methods**). Consistent
227 with bulk-eQTLs⁵⁶, fine-mapped sc-eQTLs (PIP ≥ 0.5) across cell types were highly enriched in promoter-
228 like regions, enhancers, and evolutionarily conserved regions (**Figure 4A**). Overall, we observed greater
229 enrichments for these annotations when using sc-eQTLs compared with bulk-eQTLs, however these
230 differences were not significant, likely resulting from baseline annotations not reflecting cell-type-
231 specificity. Additionally, we observed fine-mapped sc-eQTLs were less likely to be near promoter regions
232 ($P = 6.71 \times 10^{-4}$) and more distal ($P = 1.07 \times 10^{-4}$) when compared with bulk-eQTLs (**Figure 4B**),
233 suggesting that single-cell eQTL mapping can better prioritize distal regulatory elements.

234 Next, we sought to compare the enrichment of cell-type-specific candidate cis-regulatory
235 elements (cCREs), derived using single-cell omics or isolated cell types, between fine-mapped sc-eQTLs
236 and bulk-eQTLs. First, we confirmed that sc-eQTLs were enriched in cell-type-matched cCREs reflecting
237 open chromatin, enhancers, and promoters (**Figure 4C; Methods**). We observed that sc-eQTLs were
238 highly enriched in enhancer-gene links in matched cell types. Importantly, sc-eQTLs were more enriched
239 in cell-type matched open chromatin ($P = 6.77 \times 10^{-9}$), enhancers ($P = 3.40 \times 10^{-10}$) and promoters ($P =$
240 1.26×10^{-6}) compared with bulk-eQTLs after meta-analysis across cell types (**Figure 4C**). Lastly, we
241 further confirmed the accuracy of sc-eQTLs linked to their target genes by observing stronger enrichment
242 in cell-type-matched enhancer-gene links identified by SCENT⁵⁷ compared to bulk-eQTLs ($P = 3.38 \times$
243 10^{-4} ; **Figure S24**), highlighting the necessity of conducting eQTL mapping using single-cell data to
244 capture signals masked by bulk approach.

245 In summary, our analyses suggest that sc-eQTLs are enriched for distal cell-type-specific CREs
246 that are likely missed by bulk-eQTL approach.

247 sc-eQTL location predicts cell-type specificity

248 Understanding how sc-eQTLs are shared across cell types is challenging due to differential statistical
249 power between cell types. Specifically, simply counting sc-eQTLs based on their significance or fine-
250 mapping results would conclude to a high cell-type specificity of sc-eQTLs (**Figure S25**; results similar to
251 the ones reported by ref.¹⁹), but ignores the pervasive correlation of eQTL effects between cell types
252 (**Figure S26**; as observed using eQTLs from bulk cell type samples in ref.³⁷). To mitigate this, we
253 analyzed fine-mapped sc-eQTLs using *mashr*, which provides posterior effect estimates and significance
254 of effect after accounting for the effect size correlation between cell types and residual correlation due to
255 sample overlap⁵⁸ (2,012 sc-eQTLs with PIP ≥ 0.5 and significant at a local false sign rate (LFSR) < 0.05
256 in at least one cell type).

257 Using the *mashr* estimated effect sizes, we found that 67% of fine-mapped sc-eQTLs were shared
258 by sign across all 14 cell types (**Figure 5A**), suggesting their directional effect on gene expression was
259 consistent. In contrast, eQTL effect size magnitudes were less shared due to effect size heterogeneity,
260 with 15% universally shared and 9% specific (**Figure 5A**), consistent with previous findings^{10,58,59}. Cell-
261 type-specific sc-eQTLs were most common in monocytes, reflecting their difference from lymphocytes
262 such as B cells and T cells (**Figure S27**).

263 We found cell-type-specific sc-eQTLs identified were more distal from TSS compared with shared
264 sc-eQTLs (mean 102,164 vs. 53,733 bp, $P = 2.17 \times 10^{-6}$; **Figure 5B**), consistent with previous work
265 showing that distal CREs were more likely to be cell-type-specific^{60,61}. Lastly, we calculated the pairwise
266 sharing of sc-eQTL by magnitude and found cell type sharing outside expected subtype groups (**Figure**
267 **S28**). For example, we found 84% shared sc-eQTLs between effector memory CD8+ T cells and natural
268 killer (NK) cells, suggesting their shared cytotoxic effector mechanisms between adaptive and innate
269 immunity⁶².

270 To validate the specificity of cell-type-specific sc-eQTLs identified by *mashr* (in comparison with
271 a baseline simple counting approach), we first calculated the replication rate and observed that cell-type-
272 specific eQTLs after *mashr* analysis were less replicated in eQTLGen (0.60 vs. 0.77, $P = 3.11 \times 10^{-7}$) and
273 GTEx (0.33 vs. 0.47, $P = 5.19 \times 10^{-4}$) respectively, consistent with the expectation that sc-eQTL effects

274 private to a single cell type were likely masked by the bulk-eQTL study. Second, we found the cell-type-
275 specific sc-eQTLs identified by *mashr* were more distal from TSS compared to the simple counting
276 approach (mean 102,164 vs. 63,873 bp, $P = 9.56 \times 10^{-4}$), suggesting *mashr* was more powerful in
277 identifying distal cell-type-specific sc-eQTLs. Finally, we identified scATAC-seq peaks exclusive to each
278 cell type and calculated the enrichment of cell-type-specific open chromatin. We observed the specific
279 eQTLs identified by *mashr* were more enriched in cell-type-specific open chromatin in rarer cell types
280 (**Figure S29**), such as non-classical monocytes (Mon_{NC}), NK recruiting (NK_R) cells, CD4+ T cells
281 expressing SOX4 (CD4_{SOX4}), and Plasma, which reflected eQTL sharing results (**Figure S27**).

282 In summary, our analyses suggest that the genetic effect of sc-eQTLs are largely shared across
283 cell types. sc-eQTLs closer to TSS are more likely to be shared while distal sc-eQTLs are likely cell-type-
284 specific due to the different regulatory elements involved in transcription.

285 sc-eQTLs reveal cell types associated with GWAS immune traits

286 After observing that sc-eQTLs improved our ability to identify cell-type-specific eQTLs, we next
287 investigated whether sc-eQTLs can improve the interpretation of GWAS findings, which SNP-heritability
288 (h^2) tend to be concentrated in SNPs within cCREs^{55,63,64} and genes active in disease-relevant cell types
289⁶⁵⁻⁶⁷. To quantify the extent to which sc-eQTLs can characterize GWAS findings, we first evaluated the
290 fraction of h^2 explained by SNP-annotations constructed from fine-mapped sc-eQTLs in all PBMC cell
291 types and meta-analyzed S-LDSC results across 16 immune diseases and blood traits (**Table S7**). We
292 found that the union of fine-mapped sc-eQTLs across 14 cell types (3.5% of common SNPs) were
293 enriched in h^2 (2.82 ± 0.25), and explained $9.90 \pm 0.88\%$ of h^2 . Importantly, fine-mapped sc-eQTLs
294 explained more h^2 than bulk-eQTLs ($6.10 \pm 0.76\%$; **Figure 6A**) while maintaining comparable h^2
295 enrichment (2.76 ± 0.34 ; **Figure S30**), suggesting that sc-eQTLs increase the number of GWAS variants
296 that can be functionally characterized.

297 We further investigated whether h^2 was enriched within sc-eQTLs from disease-relevant cell types
298 (**Figure 6B**). We ran S-LDSC on sc-eQTL annotations built from each cell type, and individually looked
299 at their effects while conditioning on the union of fine-mapped sc-eQTLs. Overall, identified cell types
300 were consistent with known biology and previous studies leveraging cCREs and genes differentially
301 expressed. For example, we identified monocyte cell types for monocyte percentage (min $P = 1.80 \times 10^{-3}$
302 for Mon_{NC}) and major sub-cell-types of B cells and T cells for lymphocyte percentage (min $P = 4.26 \times$
303 10^{-4} for CD4_{NC}). For immune diseases, we identified various T cell subtypes for celiac disease⁶⁶ (min P
304 $= 7.65 \times 10^{-3}$ for CD4_{NC}), inflammatory bowel disease⁶⁶ (min $P = 1.34 \times 10^{-4}$ for naïve and central memory
305 CD8+ T cells (CD8_{NC})), hypothyroidism⁶⁷ (min $P = 9.91 \times 10^{-3}$ for CD8_{ET}), primary biliary cirrhosis⁶⁶ (min
306 $P = 3.45 \times 10^{-2}$ for CD8_{NC}), and rheumatoid arthritis^{66,68} (min $P = 3.43 \times 10^{-3}$ for CD8_{ET}), as well as the
307 role of NK cells for eczema⁶⁹ (min $P = 1.12 \times 10^{-2}$ for NK).

308 Altogether, these results highlight that sc-eQTLs can improve our ability to characterize GWAS
309 findings by identifying new eQTLs in disease relevant cell types.

310 sc-eQTLs prioritize candidate genes missed by bulk-eQTLs

311 To demonstrate that sc-eQTLs can prioritize GWAS candidate genes that would have been missed by
312 bulk sequencing, we present OneK1K sc-eQTLs and bulk-eQTLs results at a leading genetic risk loci
313 associated with rheumatoid arthritis (RA) ⁷⁰ in *ANKRD55-IL6ST* region ^{71,72} (**Figure 7**). We identified the
314 GWAS leading SNP rs7731626 (chr5:55444683:G>A) as the top candidate causal sc-eQTLs for *IL6ST*
315 in CD4_{NC} (PIP = 1) and CD8_{NC} T cells (PIP = 0.98), and observed significant colocalization with RA for
316 these two cell types (PP.H4 = 1, and PP.H4 = 0.99, respectively). In contrast, this SNP became null in
317 bulk-eQTL results as its eQTL effect on *IL6ST* was diluted when cell types were lumped together. We
318 further confirmed that rs7731626 is likely to be within an enhancer acting on *IL6ST* regulation in T cells
319 by observing contact between rs7731626 and *IL6ST* promoter exclusively in T cells using promoter
320 capture Hi-C (PChi-C) experimental data ⁷³, as well as H3K27ac peaks (capturing enhancer activity) at
321 this locus in naive CD4+ and CD8+ T cells ^{74,75} (**Figure 7**; see **Code and Data Availability**); the link
322 between rs7731626 and *IL6ST* in T cells has also been established by other single-cell multi-omic data
323 approaches ^{34,76–78}. We replicated the rs7731626-*IL6ST* association in CD4+ and CD8+ T cells in CLUES
324 European- and Asian-ancestry individuals (N=88, p=0.03 respectively), except rs7731626 in CD8+ T cells
325 among Europeans (p=0.3), likely due to lower sample size for detecting weaker effect as evidenced by
326 consistent effect direction. Besides, we also identified rs7731626 as both a bulk-eQTL and sc-eQTL for
327 *ANKRD55* and similar colocalization with RA (**Figure S31**), illustrating that while bulk-eQTL approaches
328 can identify strong sc-eQTL signal, they can nominate an incomplete list of candidate genes.

329 Additional colocalization results between RA GWAS and OneK1K sc-eQTLs are presented in
330 **Figure S32**. We identified 43 eGene colocalizing with RA (PP.H4 > 0.9), primarily in T and B cells
331 (consistent with literature ⁷⁹). We notably found that *EOMES* eQTLs colocalized with RA in CD8+ T cells
332 (PP.H4 = 0.97), consistent with the role of *EOMES* as a key TF for mediating immunity function in effector
333 CD8+ T cells⁸⁰. Similarly, *CD40* eQTLs colocalized with RA in Plasma cells, reflecting that *CD40* signaling
334 pathway plays an essential role in immune response in B cells ^{81,82}.

335 Altogether, these results illustrate that sc-eQTL analysis can reveal new candidate genes for
336 diseases that are masked by bulk approach.

337 Discussion

338 We developed jaxQTL, an efficient and powerful approach for large-scale eQTL mapping on single-cell
339 data using count-based models. Through simulation and real data analyses, we showed that the negative
340 binomial model was the most powerful and well-calibrated model compared with the linear and Poisson
341 models. In an application to OneK1K, we found that jaxQTL was more powerful in identifying eGenes
342 compared to tensorQTL (linear model) and SAIGE-QTL (Poisson mixed model) while exhibiting
343 comparable or better runtimes when performed using GPUs/TPUs.

344 We further leveraged jaxQTL results to characterize eGenes and their corresponding fine-mapped
345 sc-eQTLs. First, we found that eGenes are depleted of loss-of-functions variants and large-effect eQTLs,
346 consistent with previous works on bulk-eQTLs ^{49,51–53}. Second, we showed that sc-eQTLs are more distal
347 to TSS and more enriched in cell-type matched CREs compared with bulk-eQTLs, and that sc-eQTLs
348 effects are largely consistent across cell types (as observed using eQTLs from bulk cell type samples in

349 ref.³⁷), with cell-type-specificity increasing with distance to TSS. These results summarize that while bulk-
350 eQTLs identify primarily proximal regulatory effects with low cell-type-specificity (e.g., promoter), sc-
351 eQTLs allow to identify additional distal regulatory effects with medium to high cell-type-specificity (e.g.,
352 enhancer). Finally, we demonstrated that sc-eQTLs explain more heritability than bulk-eQTLs for GWAS
353 traits, suggesting that the GWAS risk variants were partially driven by eQTLs with medium to high cell-
354 type-specificity. We used an example of *ANKRD55-IL6ST* loci to demonstrate that sc-eQTLs can
355 prioritize RA-associated gene *IL6ST* missed by bulk approach. This candidate gene is well-documented
356 for its functional role on the key therapeutic target cytokine *IL6*⁸³⁻⁸⁵, and is further supported by other
357 genetic evidence such as its higher PoPs prioritization scores⁸⁶ compared with the closest gene
358 *ANKRD55* (top 1% vs 13% percentile respectively).

359 jaxQTL has several advantages compared to existing sc-eQTL methods. First, jaxQTL requires
360 no data transformation on gene expression outcomes such that it provides an eQTL effect estimate on
361 the interpretable count data scale. Second, we showed through simulations that jaxQTL outperformed
362 the linear model (used by tensorQTL) in identifying eQTLs, especially for lower expressed genes and
363 rare cell types. This will be well suited for rare cell types and precise cell states in short-read scRNA-seq
364 and low counts of isoforms transcripts in long-read scRNA-seq. Lastly, jaxQTL leverages GPU/TPU to
365 maximize efficiency in sc-eQTL mapping at population scale (N>100) while performing the permutations
366 requested in eQTL best practices²⁸. Although SAIGE-QTL similarly used a count-based model without
367 permutation calibration, jaxQTL on GPU/TPU was on average 3.7x faster than SAIGE-QTL with sample
368 size observed (N=982) in OneK1K and 1,560x faster in simulated data for dominant cell type with sample
369 size N=10,000 (mimicking the upcoming TenK10K data). Importantly, when performing ACAT-V to
370 compute gene-level P values, jaxQTL was 1.3 - 10,596x times faster than SAIGE-QTL for N=100 to
371 10,000, and displayed times comparable with the linear model of tensorQTL (with permutations).

372 Our findings have several implications for further single-cell sequencing studies and their
373 integration with GWAS. First, we demonstrated the benefits of the negative binomial model over the
374 Poisson mixed model for sc-eQTLs mapping. jaxQTL can be applied to other count data such as peak
375 reads from scATAC-seq, or extend to accommodate other molecular outcomes such as isoform ratios,
376 while efficiently accounting for the larger number of tests to perform in these datasets (e.g. ~300K of
377 ATAC-seq peaks in scATAC-seq⁸⁷ vs. ~20K genes in scRNA-seq). We thus recommend considering
378 jaxQTL with the negative binomial models for further analyses of population-scaled scATAC-seq and/or
379 multiome datasets to identify chromatin activity QTLs. Second, jaxQTL is scalable for identifying sc-
380 eQTLs in extremely large scRNA-seq datasets. As advances in the ability to multiplex samples in single-
381 cell sequencing assays is allowing generating scRNA-seq and multiome datasets in hundreds to
382 thousands of samples, we expect jaxQTL to be leveraged for analyzing datasets beyond OneK1K and
383 TenK10K. Third, we highlighted that sc-eQTL effects are more shared across cell types than previously
384 reported¹⁹. This property might motivate new sc-eQTL mapping and fine-mapping methods jointly
385 integrating all cell types to increase power. Finally, we observed that while OneK1K sc-eQTLs explained
386 a higher proportion of heritability than bulk-eQTLs for GWAS of immune traits, they did not close the
387 missing link between GWAS and eQTLs. While generation of larger scRNA-seq datasets will improve the
388 detection of distal sc-eQTLs with high cell-type-specificity, closing this gap might involve identifying sc-
389 eQTLs with *trans*-effects, generating scRNA-seq data from disease-relevant contexts (such as
390 stimulating condition⁸⁸ and developmental stage⁸⁹), or generating other types of single-cell QTLs (such

391 as splice QTLs⁹⁰, chromatin activity QTLs⁸⁷ and methylation-QTL⁹¹). In all those scenarios, jaxQTL can
392 be easily extended to efficiently analyze those datasets.

393 We note several limitations of our work. First, jaxQTL power is dependent on cell type abundance,
394 which will limit sc-eQTL power for rare cell types and precise cell states. Despite this, jaxQTL identified
395 more eGenes within rare cell types than existing methods. Second, pseudobulk approaches aggregate
396 read counts over discrete cell types, which may fail to capture dynamic contexts, thus limiting the
397 identification of dynamic sc-eQTLs^{34,35} (i.e. variants impacting gene expression within a cell type whose
398 effects vary dynamically along a continuous state). Identifying dynamic sc-eQTLs with jaxQTL could be
399 performed by identifying sc-eQTLs in more precise cell states, but further work would be required to
400 evaluate this approach. Third, our analyses were restricted to PBMCs and immune-related diseases, and
401 it is unclear if our conclusions translate to sc-eQTLs from different tissues and disease types. However,
402 ongoing release of sc-RNAseq data from brain samples will allow characterizing brain sc-eQTLs and their
403 role in psychiatric traits²⁰. Fourth, our analyses were also restricted to European individuals. Assessing
404 the transportability of our conclusions in non-European populations is a critical future research direction,
405 as different environments and genetic backgrounds impact gene regulation and disease effect sizes⁹².
406 While the recent release of a population-scaled scRNA-seq from East-Asian individuals will allow
407 identifying sc-eQTLs and characterizing their role in East-Asian populations⁹⁰, there is a need to generate
408 datasets in more diverse populations. Despite these limitations, jaxQTL provides an efficient and flexible
409 framework for eQTL mapping on single-cell data using a count-based model. Our findings enable rich
410 biological and mechanistic interpretation for disease risk loci at the cell-type level and nominate
411 therapeutic targets for complex diseases.

412

413 Declaration of interests

414 S.G. reports consulting fees from Eleven Therapeutics unrelated to the present work. The other authors
415 declare no competing interests.

416 Acknowledgments

417 This work was funded in part by the National Institutes of Health (NIH) under awards P01CA196569,
418 R01HG012133, R01CA258808, R35GM147789, R01GM140287, and R00HG010160. We thank Dr.
419 Joseph Powell for kindly sharing their processed OneK1K gene expression count matrix and genotype
420 data. We thank the ENCODE consortium for generating experimental data for epigenetic markers by cell
421 types. We thank members from the Impact of Genomic Variation on Function (IGVF) consortium QTL
422 focus group for insightful discussions on these results. We thank participants for providing feedback for
423 this work during the Computational Genomics Summer Institute (CGSI) program at UCLA under award
424 GM135043. We thank Dr. Bolun Li for providing user feedback on jaxQTL software.

425 Author Contributions

426 Z.Z., N.M., and S.G. conceived the study. Z.Z., S.G., and N.M. developed the method. Z.Z. performed
427 analyses. N.S. and A.K. prepared data and performed analyses. All authors edited and approved the
428 manuscript.

429 Web Resources

430 JAX: <https://github.com/google/jax>
431 tensorQTL: <https://github.com/broadinstitute/tensorQTL>
432 SAIGE-QTL: <https://github.com/weizhou0/qtl>
433 bedtools: <https://bedtools.readthedocs.io/en/latest/>
434 qvalue R package: <https://github.com/StoreyLab/qvalue>
435 susieR package: <https://github.com/stephenslab/susieR>
436 GTEx pipeline: <https://github.com/broadinstitute/gtex-pipeline/tree/master>
437 SLDSC software: <https://github.com/bulik/ldsc>
438 1000 Genome annotations: <https://alkesgroup.broadinstitute.org/LDSCORE/>
439 PLINK software: <https://www.cog-genomics.org/plink/2.0/>
440 mashr: <https://stephenslab.github.io/mashr/index.html>
441
442 GTEx v8 eQTL summary statistics (EUR): <https://gtexportal.org/home/downloads/adult-gtex/qtl>
443 DICE cis-eQTL summary statistics: <https://dice-database.org/>
444 eQTL catalogue: <https://www.ebi.ac.uk/eqtl/>
445 CLUES data: Gene expression data are available in the Human Cell Atlas Data Coordination Platform
446 (<https://explore.data.humancellatlas.org/projects/9fc0064b-84ce-40a5-a768-e6eb3d364ee0/project->

447 [matrices](#)) and at GEO accession number GSE174188. Genotypes are available at dbGap accession
448 number phs002812.v1.p1
449
450 GTEx v8 SuSiE fine-mapping results: <https://www.finucanelab.org/data>
451 Gene GTF file (release 84):
452 https://ftp.ensembl.org/pub/grch37/release-84/gtf/homo_sapiens/Homo_sapiens.GRCh37.82.gtf.gz
453 pLI and LOEUF score from gnomad:
454 [https://storage.googleapis.com/gcp-public-data--](https://storage.googleapis.com/gcp-public-data--gnomad/release/4.0/constraint/gnomad.v4.0.constraint_metrics.tsv)
455 [gnomad/release/4.0/constraint/gnomad.v4.0.constraint_metrics.tsv](https://storage.googleapis.com/gcp-public-data--gnomad/release/4.0/constraint/gnomad.v4.0.constraint_metrics.tsv)

456 Data and Code Availability

457 Single-cell eQTL summary statistics results produced by jaxQTL and fine-mapping results are available
458 on Zenodo:10.5281/zenodo.14624945
459
460 jaxQTL software: <https://github.com/mancusolab/jaxQTL>
461 jaxQTL analysis code: https://github.com/mancusolab/jaxqtl_analysis
462 Original OneK1k data are available at:
463 <https://www.ncbi.nlm.nih.gov/geo/query/acc.cgi?acc=GSM5901755>
464
465 We downloaded the call sets from the ENCODE portal (<https://www.encodeproject.org/>) with the following
466 identifiers: ENCFF313TWH (CD4 T cell), ENCFF635YOQ (CD8 T cell), ENCFF071MEQ (B cell),
467 ENCFF814VKT (NK cell), and ENCFF468QFA (Monocyte).

Online Methods

469 GLM and count-based eQTL models

470 Here, we describe the core generalized linear model (GLM) for a focal gene within a focal cell type c ,
 471 assuming that cell type labels for each cell have been provided. Specifically, jaxQTL models the
 472 conditional expectation of pseudobulk counts y_c (i.e. sum of read counts across cells within the cell type),
 473 given covariates X (e.g., age, sex, genotyping principal components) and a cis-genetic variant g , as

$$474 \quad E[y_c | X, g] = h(X\beta + g\beta_g + l_c),$$

475 where β are the covariate effects, β_g is the allelic effect, l_c is an offset adjusting for differences in library
 476 size, and $h(\cdot)$ is a function which maps linear predictions to expected values. Additionally, jaxQTL models
 477 the conditional variance as,

$$478 \quad \text{Var}[y_c | X, g] = \text{Var}_\alpha(h(X\beta + g\beta_g + l_c)),$$

479 where $\text{Var}_\alpha(\cdot)$ corresponds to a variance function determined by the specified likelihood (e.g., Poisson,
 480 negative binomial) allowing for an overdispersion parameter α if required (e.g., negative binomial)^{45,93}.

481 We fit a null GLM using iteratively reweighted least squares (IRWLS). Namely, assuming there is
 482 no genotype effect (i.e. $\beta_g = 0$), the update step for covariate effects β at the $t + 1$ iteration can be
 483 computed by solving a linear system given by,

$$484 \quad X^T W_t X \beta_{t+1} = X^T W_t (e_t + X\beta_t),$$

485 where $e_t \propto (y - \mu_t)$ are the “working residuals”, $\mu_t = h(X\beta_t + l_c)$, and W_t are the GLM weights
 486 proportional to the reciprocal of the conditional variance. To solve this linear system, jaxQTL allows for
 487 different solvers (e.g., QR, Cholesky, and conjugate gradient), however in practice we found Cholesky to
 488 outperform other approaches.

489 While both the Wald test and score test are implemented in the software, jaxQTL employs the
 490 score test in assessing the nonzero cis-SNP effect β_g on y_c for its improved computational efficiency⁹⁴.
 491 Specifically, we first fit the null GLM model described above. Next, jaxQTL uses a block matrix approach
 492 to efficiently compute score test statistics for all p cis-SNPs in a focal gene. Let $d = \text{diag}(\widehat{G}^T W \widehat{G})$ be a
 493 length p vector, then the vector of test statistics Z is given by,

$$494 \quad Z = (\widehat{G}^T W e) \oslash d^{1/2},$$

495 where \widehat{G} is the weighted residualized genotype obtained by $\widehat{G} = G - X(X^T W X)^{-1} X^T W G$, $d^{1/2}$ is the
 496 element-wise square-root, and \oslash is element-wise division.

497 To adjust for multiple testing corrections in eGene discovery, jaxQTL provides gene-level P values
 498 calibrated by a permutation-based Beta-approximation approach, which is similarly implemented in
 499 FastQTL and tensorQTL software^{28,29}. To infer beta distribution parameters, we applied natural gradient
 500 descent using second order approximation to ensure parameters stay on the manifold (i.e. > 0)⁹⁵. Lastly,
 501 we controlled the false discovery rate (FDR) and identified eGenes using these gene-level P values.

502 We implemented jaxQTL in Python to enable *just-in-time* (JIT) compilation through the JAX
503 package (**Web Resources**), which generates and compiles heavily optimized C++ code in real-time and
504 operates seamlessly on CPU, GPU, or TPU (**Code Availability**).

505 Analysis of OneK1K single-cell data

506 We obtained 1,267,768 PBMC blood cells for 14 cell types from $N = 982$ healthy individuals of European
507 ancestry in the OneK1K cohort¹⁹. Each donor has an average of 1,291 cells (range 62-3,501). Each cell
508 type has a varying number of donors due to sampling variance (**Table S2**). For sc-eQTL mapping, we
509 created pseudobulk count data for each of the pre-annotated 14 cell types. After retaining genes with
510 sample-coverage (i.e., fraction of non-zero expression read counts) in at least 1% of the population for
511 each cell type, we performed sc-eQTL mapping for an average of 16,096 genes per cell type (**Table S2**).
512 To establish a baseline for comparison, we created “bulk” data by summing all read counts across cell
513 types for every gene and identified bulk-eQTLs using jaxQTL.

514 We first aimed to benchmark between different sc-eQTL models, including linear, negbinom, and
515 Poisson. For negbinom and Poisson, we calculated individual library size in each cell type, i.e., the offset
516 term in the model, by summing read counts across all genes per individual. For the linear model, we
517 normalized gene expression read counts between individuals by TMM approach and then normalized
518 across individuals by rank-based inverse normal transformation, as performed in GTEx¹⁰. We
519 implemented all three models using a score test in jaxQTL.

520 For genotype data, we retained 5,313,813 SNPs with imputation INFO score >0.8 , $MAF > 0.05$,
521 and Hardy Weinberg equilibrium (HWE) $P > 1e-6$. Genotype PCs were calculated using 459,603 LD-
522 pruned SNPs with $INFO > 0.9$, $MAF > 0.01$, and $HWE P > 1e-6$. Across all sc-eQTL models, we adjusted
523 covariates including age, sex, first six genotype PCs, and two expression PCs computed in each cell
524 type. We defined the cis-window size as $\pm 500\text{kb}$ (total 1Mb) around TSS. We downloaded the gene
525 annotation GTF file (Homo_sapiens.GRCh37.82) and collapsed it to a single transcript model using
526 “collapse_annotation.py” from GTEx analysis pipeline (**Web Resources**)¹⁰. We controlled gene-level
527 FDR at 0.05 per cell type using the qvalue method on gene-level P values through *qvalue* R package
528 (**Web Resources**)⁹⁶. eGenes were identified by $qvalue < 0.05$. We used genome build hg19 for all
529 variants and gene annotations.

530 To benchmark with other existing software, we compared the eGenes results of jaxQTL against
531 tensorQTL²⁹ and SAIGE-QTL³⁶. We first restricted genes to sample-coverage $> 10\%$ as in ref.³⁶ and
532 obtained their SAIGE-QTL eGenes results³⁶. Then we applied FDR control on this subset of genes to
533 call eGenes for jaxQTL-negbinom. Similarly, we performed sc-eQTL mapping using tensorQTL on this
534 set of genes (**Web Resources**). We note that the tensorQTL results we report are different from
535 tensorQTL results reported in ref.³⁶, as we sum pseudobulk counts (following GTEx recommended
536 guidelines to transform counts from bulk RNA-seq¹⁰) rather than averaging them. All reported P values
537 are two-sided unless specified otherwise.

538 Simulations

539 To evaluate the performance of the jaxQTL-linear, jaxQTL-negbinom, jaxQTL-Poisson, tensorQTL
540 (linear), and SAIGE-QTL (Poisson mixed effect) models, we first simulated read counts y_{ij} for individual
541 i in cell j for a focal gene under the Poisson mixed effect model, given by:

$$542 \log(E(y_{ij} | g_i, u_i, l_{ij})) = \beta_0 + u_i + g_i \beta_g + \log(l_{ij}),$$

543 where β_0 is a baseline intercept, $u_i \sim N(0, \sigma^2_u)$ is the random intercept for individual i that induces within-
544 sample correlation across cells, g_i is genotype with effect-size $\beta_g \sim N(0, h^2_{cis})$ where h^2_{cis} is cis-SNP
545 heritability. To reflect the cell-wise and individual-wise read counts (i.e., library size l_{ij}) observed in
546 scRNA-seq data, we sampled l_{ij} from empirical values observed in OneK1K data. To fit pseudobulk
547 linear, negbinom, and Poisson models, we created pseudobulk counts as $y_i = \sum_j y_{ij}$ and library size as
548 $l_i = \sum_j l_{ij}$. We varied the baseline expression β_0 , cis-SNP heritability h^2_{cis} , the random intercept variance
549 σ^2_u , MAF, and sample size N . Given fixed β_0 values, we obtained varying sample-coverage across
550 simulation replicates and calculated the average simulated sample-coverage (**Figure 1**; **Figure S4-8**).

551 To evaluate the performance under model misspecification, we simulated single-cell read counts
552 from the standard Poisson model assuming no within-individual correlation between cells, i.e., $\sigma^2_u = 0$.
553 In each scenario, we performed a score test for association between simulated gene expression and
554 genotype after fitting jaxQTL-linear, jaxQTL-Poisson, jaxQTL-negbinom, and SAIGE-QTL models.
555 Different from the score test in jaxQTL-linear, tensorQTL reports Wald test statistics. For the linear models
556 (jaxQTL-linear and tensorQTL), we normalized pseudobulk counts by rank-based inverse normal
557 transformation^{10,97}. Each simulation had 500 replicates.

558 Replication of sc-eQTLs

559 To validate sc-eQTLs identified by jaxQTL-negbinom, we performed replication analysis using
560 jaxQTL on two independent cohorts from CLUES study⁴⁷. We obtained scRNA-seq for $N=256$ individuals
561 of European and Asian ancestry (see **Web resources**). We removed 50 control individuals from the
562 ImmVar study, 2 outliers detected through a PCA analysis and 2 male individuals from the remaining
563 based on ref⁹². After intersecting with genotype data, we retained 88 European- and 88 Asian-ancestry
564 individuals for replication analysis. Of these, 65 and 67 individuals were diagnosed with systemic lupus
565 erythematosus (SLE) but were not in active state of disease flare. We matched 7 cell types in CLUES
566 with 14 cell types in OneK1K. We performed analysis in European and Asian individuals separately. For
567 lead SNP-eGene pairs identified by jaxQTL-negbinom, we fitted negbinom model using jaxQTL in CLUES
568 cell types. We adjusted for age, sex, first six genotype PCs, SLE status, and batch numbers in sc-eQTL
569 model. For each cell type, we reported the fraction of pairs replicated at $FDR < 0.05$ using *qvalue* R
570 package⁹⁶. To compare sc-eQTL effect size estimated by jaxQTL in CLUES and OneK1K samples
571 adjusting for fitted count scale differences, we calculated an adjusted slope estimate as $\tilde{\beta} \propto \hat{\beta} w$ where
572 $w \approx \sqrt{2p(1-p)}$ after accounting for weights in the GLM. Lastly, we compared results reported in the
573 original OneK1K linear-model based analyses to demonstrate directional consistency in sc-eQTL effect
574 estimates¹⁹.

575 We further investigated the replication of lead SNP-Gene pairs in eQTLs identified by previous
576 bulk-eQTL and sc-eQTL studies (see **Web resources**). For bulk-eQTL studies, we downloaded 1) cis-
577 eQTL results from European whole blood samples in GTEx v8 (N=588)¹⁰; 2) cis-eQTL summary statistics
578 results from FACS-sorted PBMC immune cell types in DICE study (N=91)⁴⁸. For sc-eQTL study, we
579 downloaded cis-eQTL summary statistics from PBMC scRNA-seq data in CLUES study curated by eQTL
580 catalogue (N=193)^{47,98}. All these prior results are based on the linear model approach when performing
581 eQTL mapping. Again we reported the fraction of pairs replicated at FDR < 0.05 within each cell type.

582 Computational runtime

583 To evaluate the computational runtime of jaxQTL on cis-eQTL mapping in comparison with other
584 software, we randomly selected 50 genes from chromosome 1 with sample-coverage > 1% in CD4_{NC},
585 B_{IN}, and Plasma cells observed in OneK1K. To benchmark the performance across different sc-eQTL
586 sample sizes, we performed downsampling to create gene expressions for N=100, 300, 500, and 700
587 individuals. Moreover, we performed upsampling for the expected TenK10K cohort²¹. Specifically, we
588 sampled N=10,000 individuals using the single-cell data matrix. Assuming each individual has a total of
589 5,000 cells as expected in TenK10K, we sampled the number of cells per person proportionally as
590 observed for these three cell types. Then we created pseudobulk data for jaxQTL and tensorQTL.

591 Fine-mapping on sc-eQTLs

592 To identify causal eQTL for every eGene, we performed fine-mapping using SuSiE summary statistics
593 approach for eGenes identified by sc-eQTL and bulk-eQTL approach (both jaxQTL-negbinom). We
594 excluded eGenes in the *MHC* region (chr6: 25Mb-34Mb) with complex LD patterns and the *MAPT* region
595 (chr17: q21.31) with complex inversion and duplication^{99,100}. For optimal statistical power, we first used
596 jaxQTL-negbinom to compute all pairwise summary statistics for cis-SNPs in every eGene. We calculated
597 the in-sample LD correlation matrix for cis-SNPs \hat{R} after projecting out the covariates effect under the
598 GLM weights. Specifically for negbinom model results, we calculated a weighted residualized G by $\hat{G} =$
599 $G - X(X^T W X)^{-1} X^T W G$, followed by computing $\hat{R} = D^{-1/2} \hat{G}^T W \hat{G} D^{-1/2}$, where $D = \text{diag}(\hat{G}^T W \hat{G})$ and W is
600 the individual weights calculated after fitting the null model.

601 Enrichment analysis on sc-eQTLs

602 We downloaded annotations from the LDSC baseline model and selected 12 annotations of promoter-
603 like regions, enhancers, conserved regions, and epigenetic markers (**Web Resources**). For cell-type
604 matched candidate cis-regulatory elements (CREs), we downloaded CRE peaks in PBMC cells identified
605 by scATAC-seq¹⁰¹. We extracted CREs from cell types matched with cell types in OneK1K based on
606 labels and marker genes (**Table S8**). For enhancers and promoters, we collected 33 samples for 6 cell
607 types from EpiMap and used *bedtools* to merge peak regions from different samples in the same cell
608 type (**Table S9**). Lastly, to interrogate the accuracy of sc-eQTL linked to target genes, we obtained the
609 enhancer-gene links identified by SCENT⁵⁷ in B cells, T/NK cells, and Myeloid cells. Cell types were
610 matched based on labels (**Table S10**). We removed ENCODE promoter-like regions from SCENT peaks
611 to retain putative enhancer regions.

612 For enrichment analysis on scATAC-seq, EpiMap enhancers, and promoters, we created
613 annotations for cis-SNPs taking the value of 1 if falling within the CRE region and 0 otherwise. For every
614 eGene, we performed logistic regression similar to torus¹⁰² by fitting $\text{logit}(PIP_{k,j}) = \beta_0 + \beta_{k,a} a_{k,j}$, where
615 j denotes cis-SNPs in eGene k and their annotation a . To obtain a single enrichment score for every
616 annotation in a cell type, we performed a fixed effect meta-analysis using fitted slopes and their standard
617 errors across all eGenes. Specifically, the meta-analyzed slope over eGenes is $(\sum_k \beta_{k,a} / W_{k,a}) / (\sum_k W_{k,a})$
618 with variance $1 / \sum_k W_{k,a}$, where $W_{k,a} = 1 / SE(\beta_{k,a})^2$. When comparing sc-eQTLs against bulk-eQTLs
619 enrichment, we meta-analyzed summary statistics across cell types.

620 To calculate the enrichment of sc-eQTLs in enhancer-gene pairs identified by SCENT, we defined
621 the enrichment score for every eGene as:

$$622 \quad \text{Score}_{eGene} = \frac{\text{Number of causal SNP in annotation}_{eGene} / \text{Number of cis - SNP in annotation}_{eGene}}{\text{Number of causal SNP}_{eGene} / \text{Number of cis - SNP}_{eGene}}$$

623 Then we calculated the enrichment for each cell type by taking an average of Score_{eGene} . To evaluate
624 the uncertainty of this mean enrichment score, we calculated the variance of this mean enrichment by
625 bootstrapping 1,000 iterations.

626 Cell type sharing of sc-eQTLs

627 To investigate cell type specificity or sharing of sc-eQTLs, we performed the *mashr* analysis on 2,256
628 fine-mapped sc-eQTL ($PIP \geq 0.5$) with complete summary statistics across 14 cell types⁵⁸ (**Web**
629 **Resources**). We first constructed a “finemap sc-eQTL” Z score matrix of size 2,256 x 14. To estimate
630 residual covariance between cell types due to sample overlap, we constructed a null sc-eQTL matrix
631 (21,542 x 14) by randomly sampling from 2 SNPs in every gene with $\max |Z| < 2$ across all cell types.

632 Following the instructions described elsewhere⁵⁸, we used a data-driven approach to estimate
633 the covariance matrix of the sc-eQTL effect. In brief, we first used the “finemap sc-eQTL” matrix to create
634 27 candidate covariance matrices including empirical covariance of Z score, 5 rank-1 approximation to
635 the covariance matrix, rank-5 approximation, and 19 canonical covariance matrices created by
636 *cov_canonical()*. Then we applied *cov_ed()* to estimate the covariance pattern by extreme deconvolution.
637 Lastly, we estimated the mixture weight by fitting the *mashr* model on the null sc-eQTL matrix using 27
638 covariance patterns and residual covariance. Lastly, we fitted *mashr* on the “finemap sc-eQTL” matrix to
639 obtain posterior effect estimates and local false sign rate (LFSR) using the mixture estimates from above.
640 Since we used the Z score model of *mashr*, we converted the posterior estimate back to the effect scale
641 by multiplying their standard errors as described elsewhere⁵⁸.

642 To count for sc-eQTL sharing, we first selected 2,012 sc-eQTLs with LFSR < 0.05, which was
643 similar to FDR control. For each significant sc-eQTL, we called the cell type with the strongest *mashr*
644 effect size as discovery cell type. We considered two types of eQTL sharing: 1) “share by sign” means
645 the other cell type shared the sign of effect with the discovery cell type; 2) “share by magnitude” means
646 conditioning on “share by sign”, the magnitude was within a factor of 2 compared to the discovery cell
647 type.

648 For enrichment analysis of scATAC-seq peaks, we first used *bedtools subtract -A* recursively to
649 identify peaks exclusive to each cell type, i.e., cell-type-specific peaks. Then we calculated the
650 enrichment score using:

$$651 \quad \text{Enrichment}_{CT} = \frac{\text{Number of CT-specific eQTLs in Annot}_{CT} / \text{Number of analyzed eQTLs in Annot}_{CT}}{\text{Number of CT-specific eQTLs} / \text{Total number of analyzed eQTLs}},$$

652 where CT refers to cell type and Annot_{CT} is cell-type-specific peaks. To obtain standard errors for the
653 enrichment, we performed bootstrapping with 1,000 iterations on the cell type labels for CT-specific
654 eQTLs.

655 Integration sc-eQTLs with GWASs

656 To assess the overlap between sc-eQTL and GWAS risk variants, we performed an S-LDSC analysis on
657 16 GWAS results for blood and immune-related traits (**Web resources; Table S7**). Firstly, we created
658 annotations using SNPs in credible sets of fine-mapped eGenes from 14 cell types (as recommended in
659 ref.⁹¹). We constructed three sets of annotations for 1) cell-type sc-eQTL: a union of credible sets of
660 eGenes per cell type; 2) sc-eQTL_union: a union of credible sets from 1) across all cell types; 3) bulk-
661 eQTL: credible sets of eGenes in bulk-eQTL results. Then we annotated SNPs using European
662 individuals from 1000 Genome Project and performed S-LDSC analysis using these annotations (**Web**
663 **resources**). To estimate heritability, we used baseline-LD v2.2 model (96 annotations) as recommended
664 in ref.¹⁰³ to obtain estimates reducing biases from MAF- and LD-dependent architectures. To identify the
665 likely causal cell types associated with each GWAS trait, we fitted the baseline model v1.2 (53
666 annotations) to optimize statistical power as recommended in ref.¹⁰⁴. To account for background non-cell-
667 type-specific eQTLs in the baseline model, we construct an additional annotation by taking a union of
668 fine-mapped SNPs in 95% credible sets from SuSiE results across 49 GTEx tissues (**Web resources**)
669 and sc-eQTL_union from our OneK1K results in order to identify cell-type-specific effects. We focused
670 on two metrics: 1) the proportion of heritability explained by each annotation $h^2(C)$ from the baseline-LD
671 v2.2 model result, and 2) the standardized coefficient τ_c^* calculated by:

$$672 \quad \tau_c^* = \tau_c \text{sd}(\tau_c) / (h^2 / M),$$

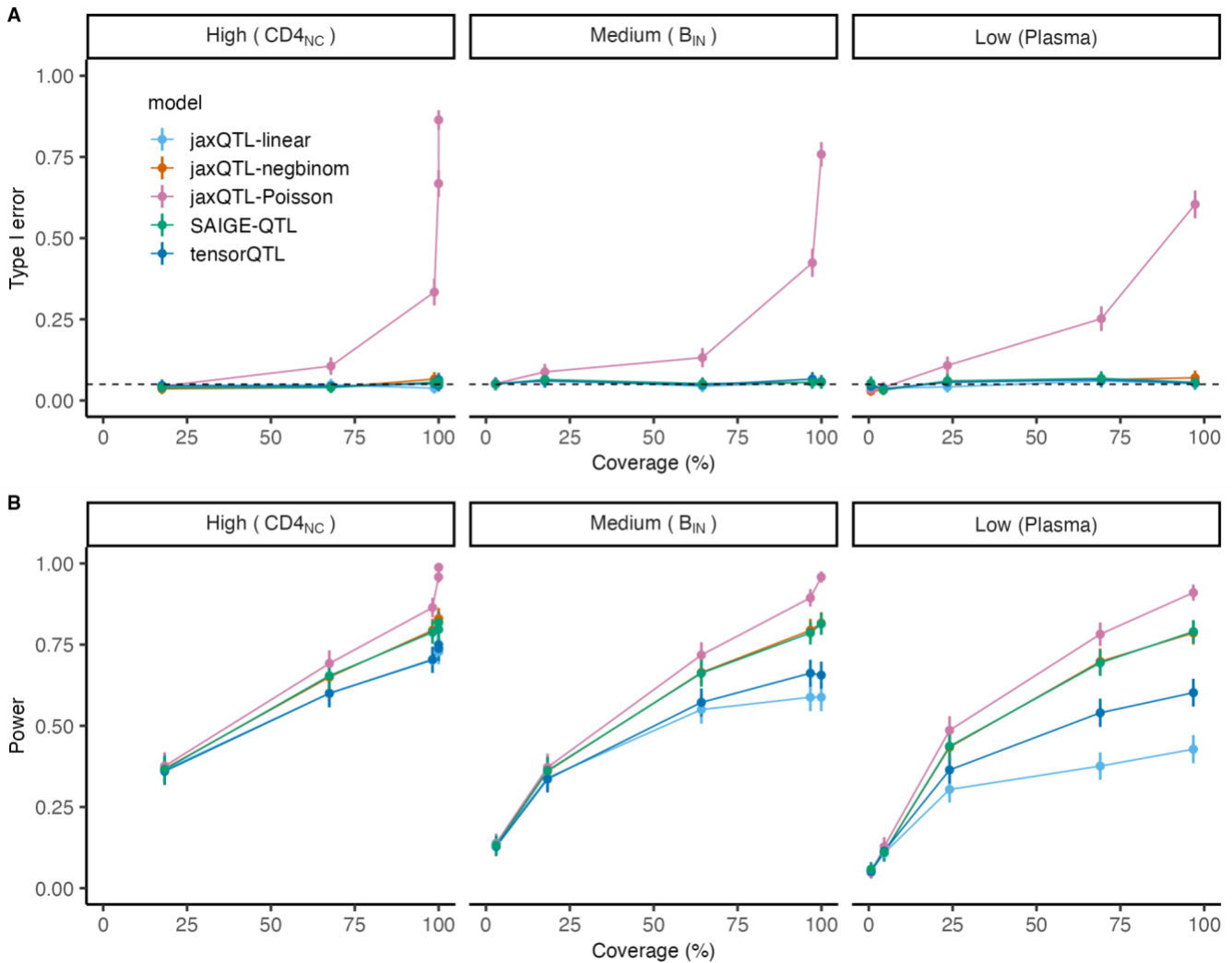
673 where τ_c , $\text{sd}(\tau_c)$, h^2 were estimated from the baseline model and M was the total number of SNPs that
674 h^2_g was computed on ($M = 5,961,159$) using 1000 Genome Project and baseline v1.2 model. Here τ^* is
675 the change in per-SNP heritability with one standard deviation increase in annotation, which makes it
676 comparable between annotations and GWAS traits. The P values are one-sided hypothesis test for $\tau^* >$
677 0.

678

679 **Figures**

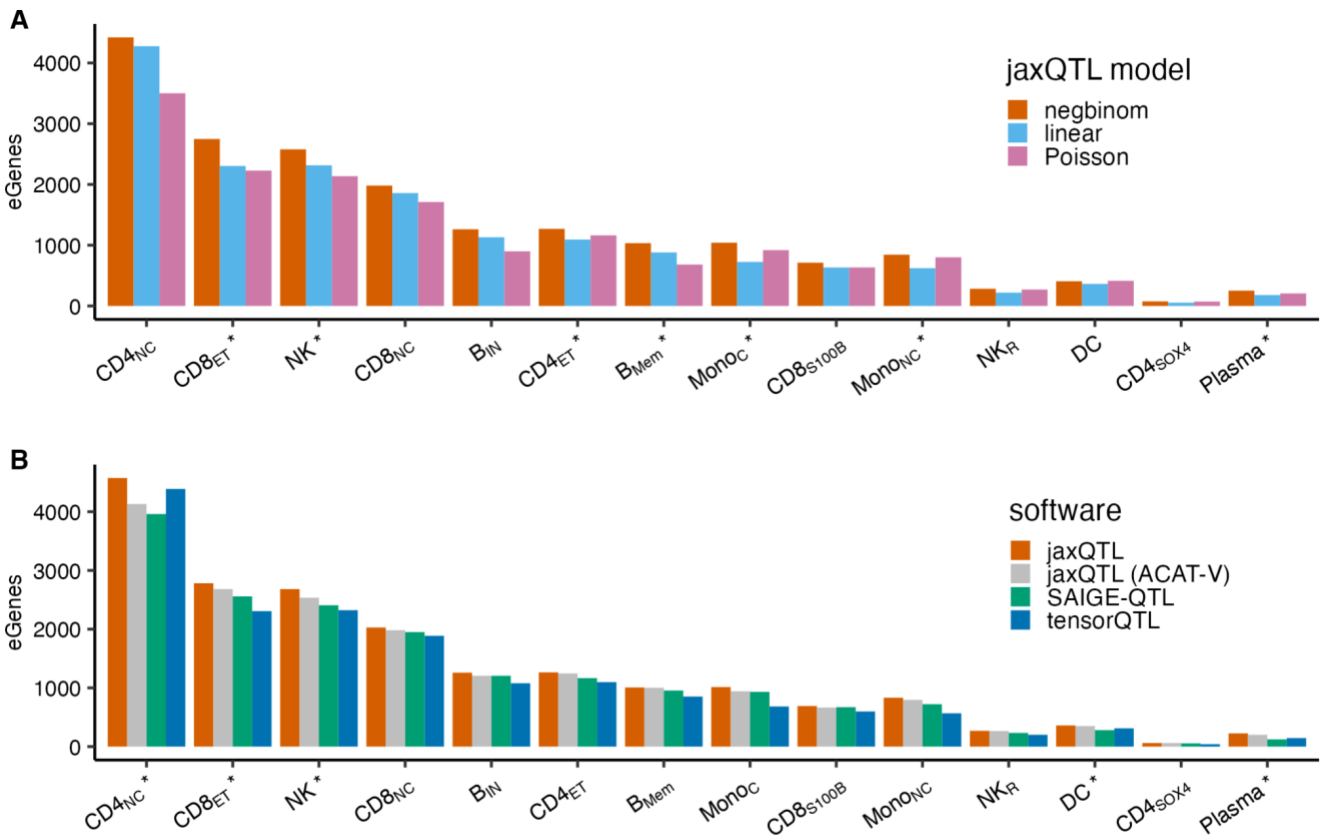
680 **Figure 1: Negative binomial outperforms other models in identifying sc-**
 681 **eQTLs in realistic simulations**

682 We simulated single-cell read counts using library size observed in three cell types (CD4_{NC}, B_{IN}, Plasma)
 683 representing different levels of cell type proportions (high, medium, low). We reported the type I error rate
 684 ($h^2_{cis} = 0$) **(A)** and power **(B)** of jaxQTL-linear, jaxQTL-negbinom, jaxQTL-Poisson, SAIGE-QTL, and
 685 tensorQTL models across different sample-coverage (i.e., percentage of non-zero expression read
 686 counts). We fixed cis-heritability $h^2_{cis} = 0.05$, random intercept variance σ^2_u (modeling similarity of cell
 687 read counts within the same person) = 0.2, sample size = 1,000, and MAF = 0.2; results when varying
 688 these parameters are reported in **Figures S5-S8**. Error bars represent 95% confidence intervals (CIs)
 689 estimated from 500 replicates. The dashed line in **(A)** represents a type I error of 0.05. SAIGE-QTL
 690 assumes single-cell counts while the rest assumes pseudobulk counts.



692 Figure 2: jaxQTL improves power for eGene discovery in the OneK1K
 693 dataset.

694 We compared eGene findings in OneK1K across models and software at FDR < 0.05. **(A)** For model
 695 comparison, we reported the number of eGenes identified by jaxQTL-negbinom, jaxQTL-linear, and
 696 jaxQTL-Poisson for genes with sample-coverage > 1%. **(B)** For software comparison, we reported the
 697 number of eGenes identified by jaxQTL (negbinom), jaxQTL (use ACAT-V instead of permutation
 698 method), tensorQTL, and SAIGE-QTL for genes with sample-coverage > 10% of individuals. The
 699 asterisks denote the cell type in which jaxQTL (negbinom) identified more eGenes compared with the
 700 linear model in **(A)** or SAIGE-QTL in **(B)** after Bonferroni correction. See details of description on cell
 701 types in **Table S2**. Numerical results are reported in **Table S3, S4**.
 702



703
 704
 705
 706
 707
 708
 709
 710
 711
 712

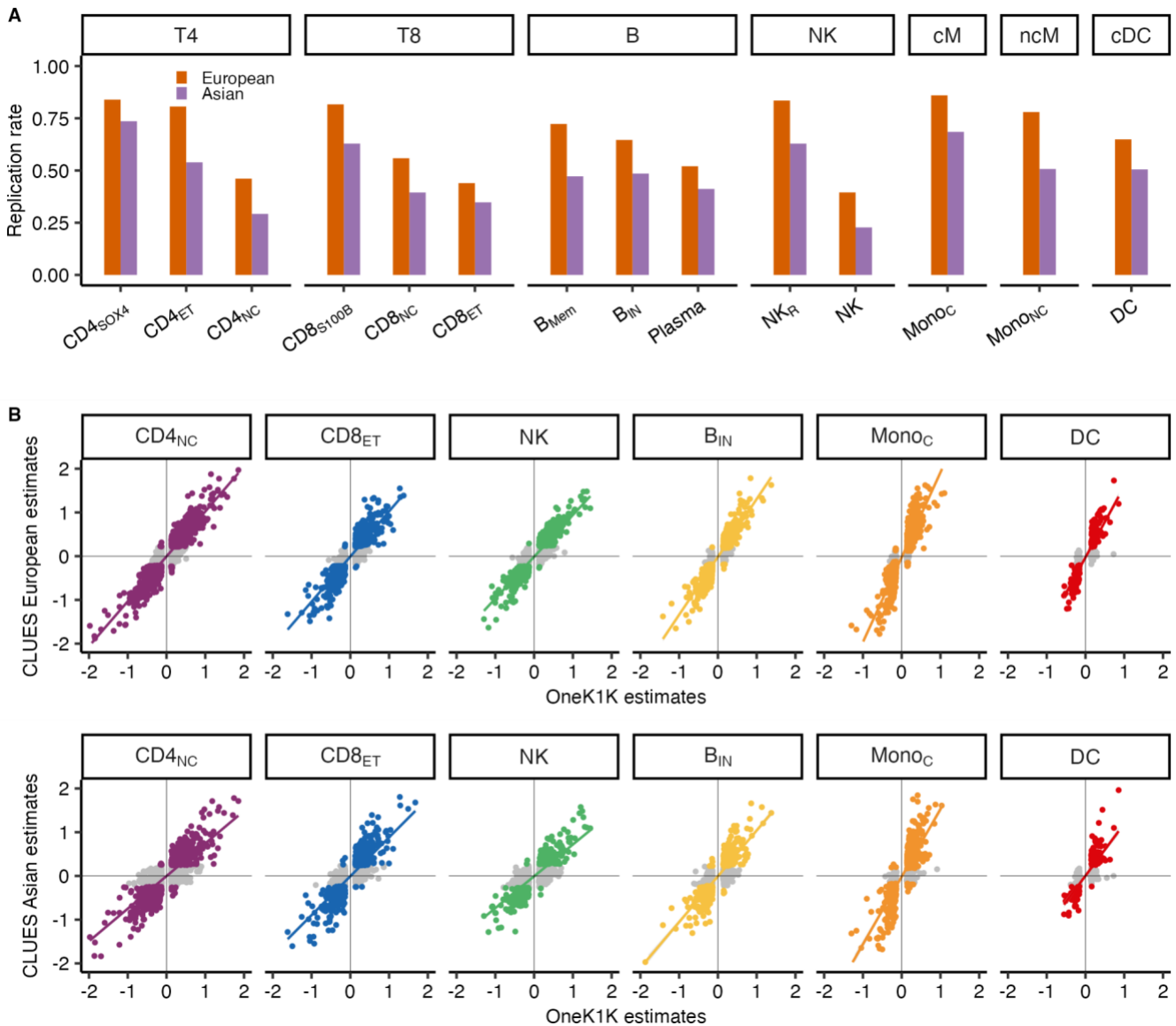
713

Figure 3: jaxQTL sc-eQTLs replicate in European and Asian samples

714

We performed replication analysis for 18,907 sc-eQTLs identified by jaxQTL in CLUES study. **(A)** Of the lead SNP-eGene pairs found in matched cell types (panels) among 88 European- and 88 Asian-ancestry individuals (14,229 and 13,579 sc-eQTLs respectively), we reported the replication rate at FDR < 0.05 by ancestry. **(B)** We plotted the adjusted sc-eQTL effect estimated by jaxQTL in CLUES versus OneK1K samples (see **Methods**). Colored points are pairs replicated at FDR < 0.05 in CLUES samples and grey points are otherwise. 35 and 20 pairs with absolute adjusted sc-eQTL effect estimate > 2 were truncated for visualization (see complete results in **Figure S16, S17** and **Table S5**). The colored line in **(B)** is a fitted linear regression line with a 95% confidence band. T4: CD4+ T cells; T8: CD8+ T cells; NK: natural killer cells; cM: CD14+ conventional monocytes; ncM: CD16+ unconventional monocytes; cDC: conventional dendritic cells.

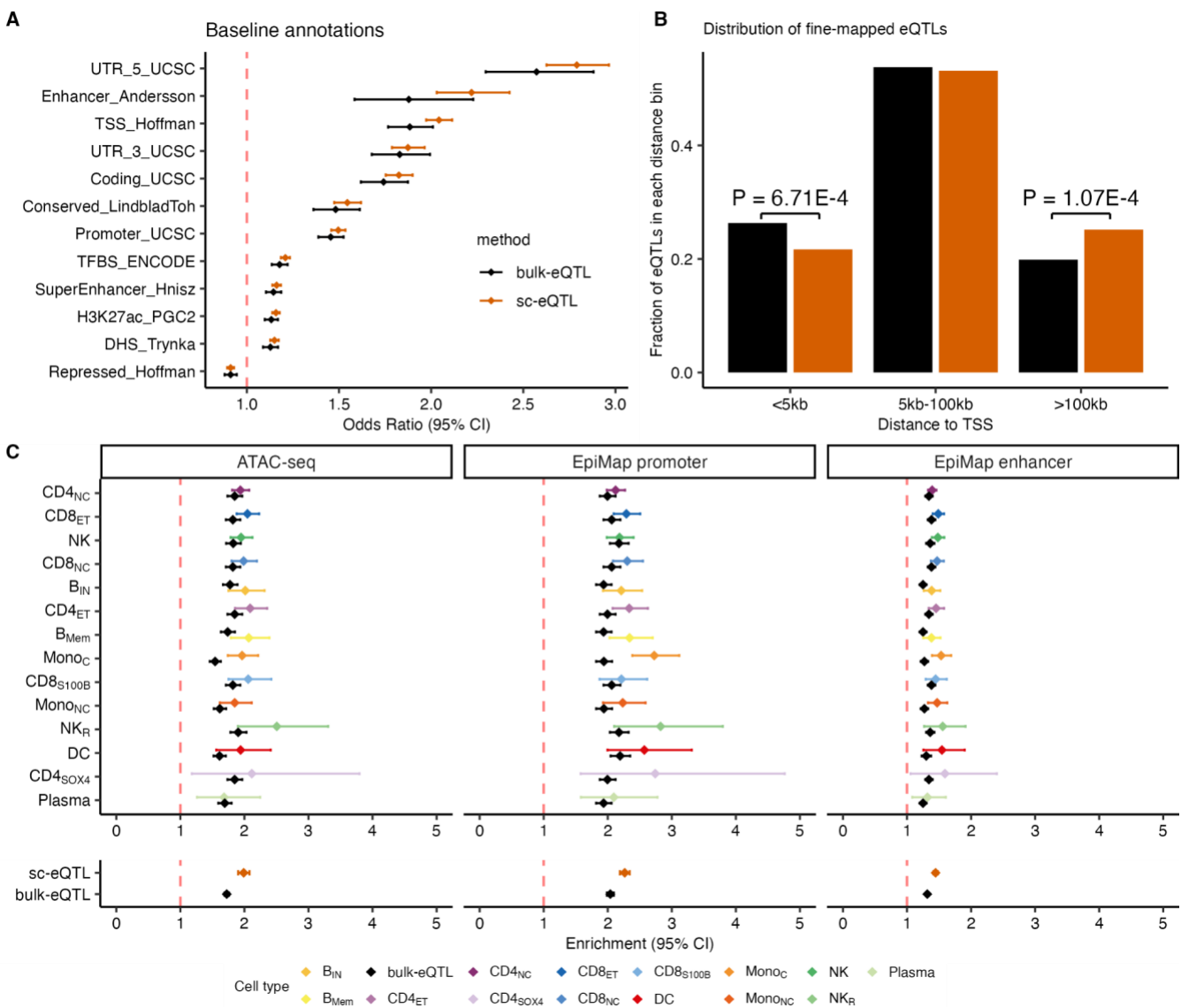
723



724

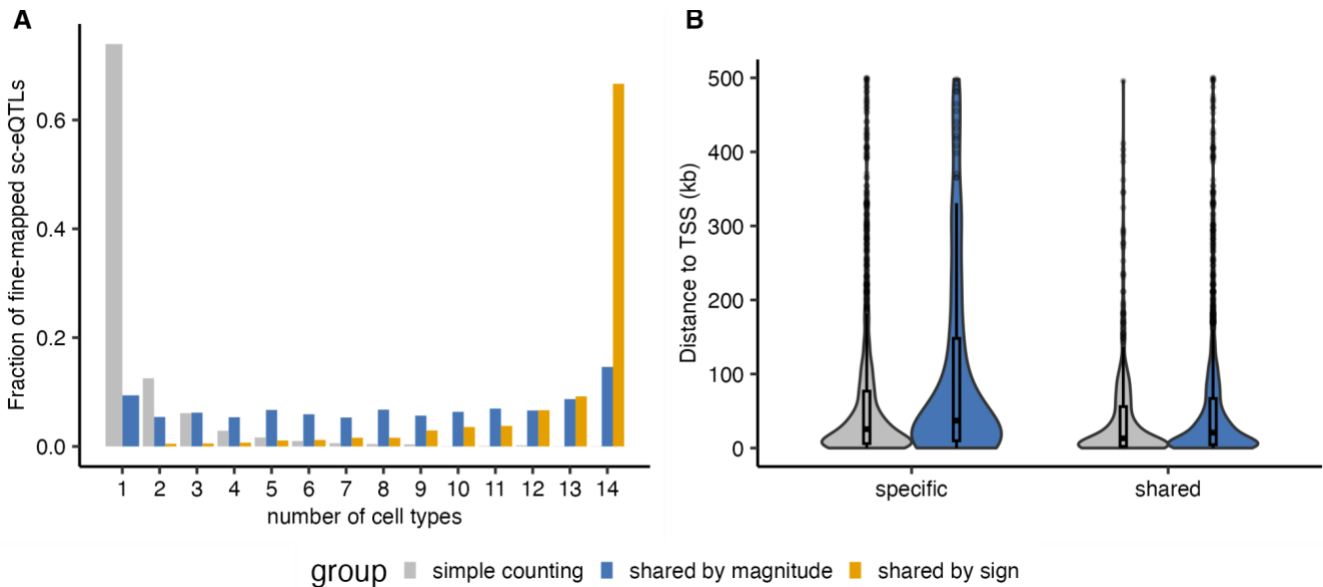
725 **Figure 4: sc-eQTLs are more enriched in cell-type-matched CREs than**
 726 **bulk-eQTLs**

727 We performed enrichment analysis of sc-eQTLs and bulk-eQTLs using their fine-mapping results and
 728 diverse annotations. **(A)** We report the odds ratio for eQTLs enrichment within 12 S-LDSC representative
 729 baseline annotations (see **Methods**). **(B)** For fine-mapped sc-eQTLs with $PIP \geq 0.5$, we report the fraction
 730 of fine-mapped eQTLs falling in three distance to TSS bins. **(C)** We report the enrichment in sc-eQTLs
 731 per cell type and bulk-eQTLs within 3 types of cell-type-specific functional annotations; we report meta-
 732 analysis results across 14 cell types at the bottom of each dataset. Error bars represent 95% CIs.
 733 Numerical results are reported in **Tables S11-14**.
 734



737 **Figure 5: sc-eQTL location predicts cell-type specificity**

738 We investigated sc-eQTL sharing across cell types by performing *mashr* analysis⁵⁸ on 2,012 OneK1K
739 sc-eQTLs fine-mapped in at least one cell type; as a baseline, we also investigated sc-eQTL sharing by
740 simple counting approach. **(A)** We report the fraction of sc-eQTL shared across different numbers of cell
741 types using three approaches: a simple counting approach, *mashr* estimates of sharing by magnitude
742 (i.e., the magnitude of effect size is within a factor of 2 compared to the strongest signal), *mashr* estimates
743 of sharing by sign (i.e. the sign of effect size is shared with this discovery cell type, i.e., the cell type with
744 the strongest signal). **(B)** We report the distance to TSS for sc-eQTLs identified as cell-type-specific or
745 shared in at least 2 cell types using a simple counting approach and *mashr*. The median value of
746 distances is displayed as a band inside each box; boxes denote values in the second and third quartiles;
747 the length of each whisker is 1.5 times the interquartile range, defined as the height of each box.
748 Numerical results are reported in **Tables S15**.
749



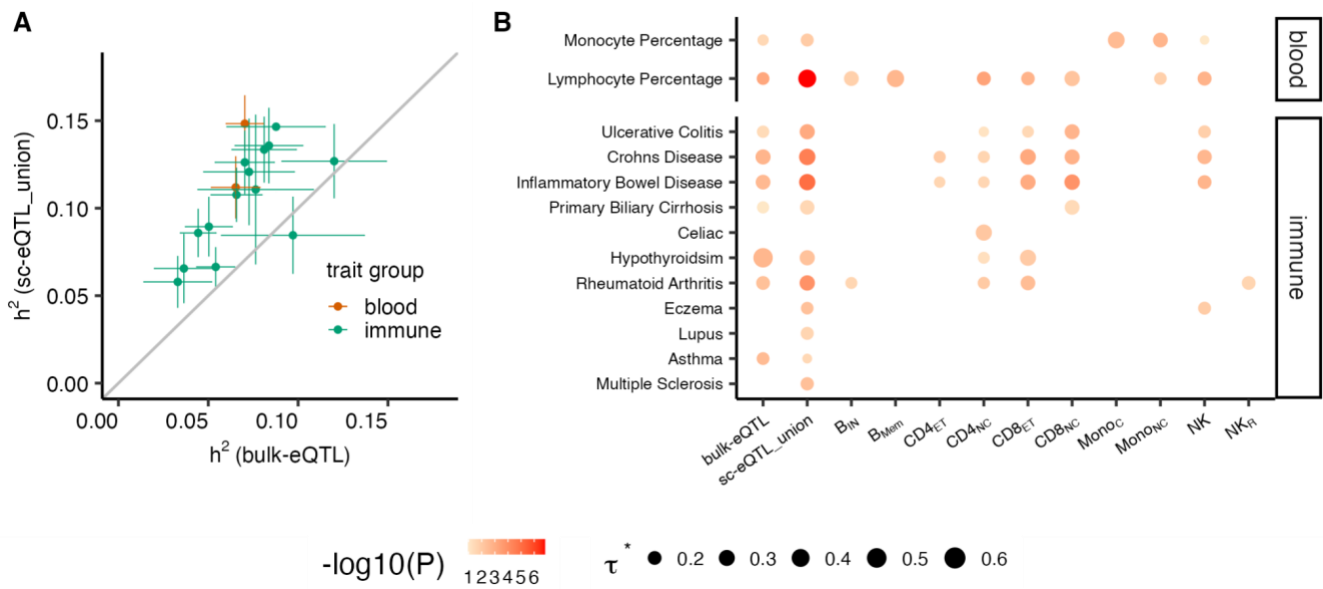
750

751

752

753 Figure 6: sc-eQTLs explain more heritability than bulk-eQTLs for
 754 immune-related GWAS traits.

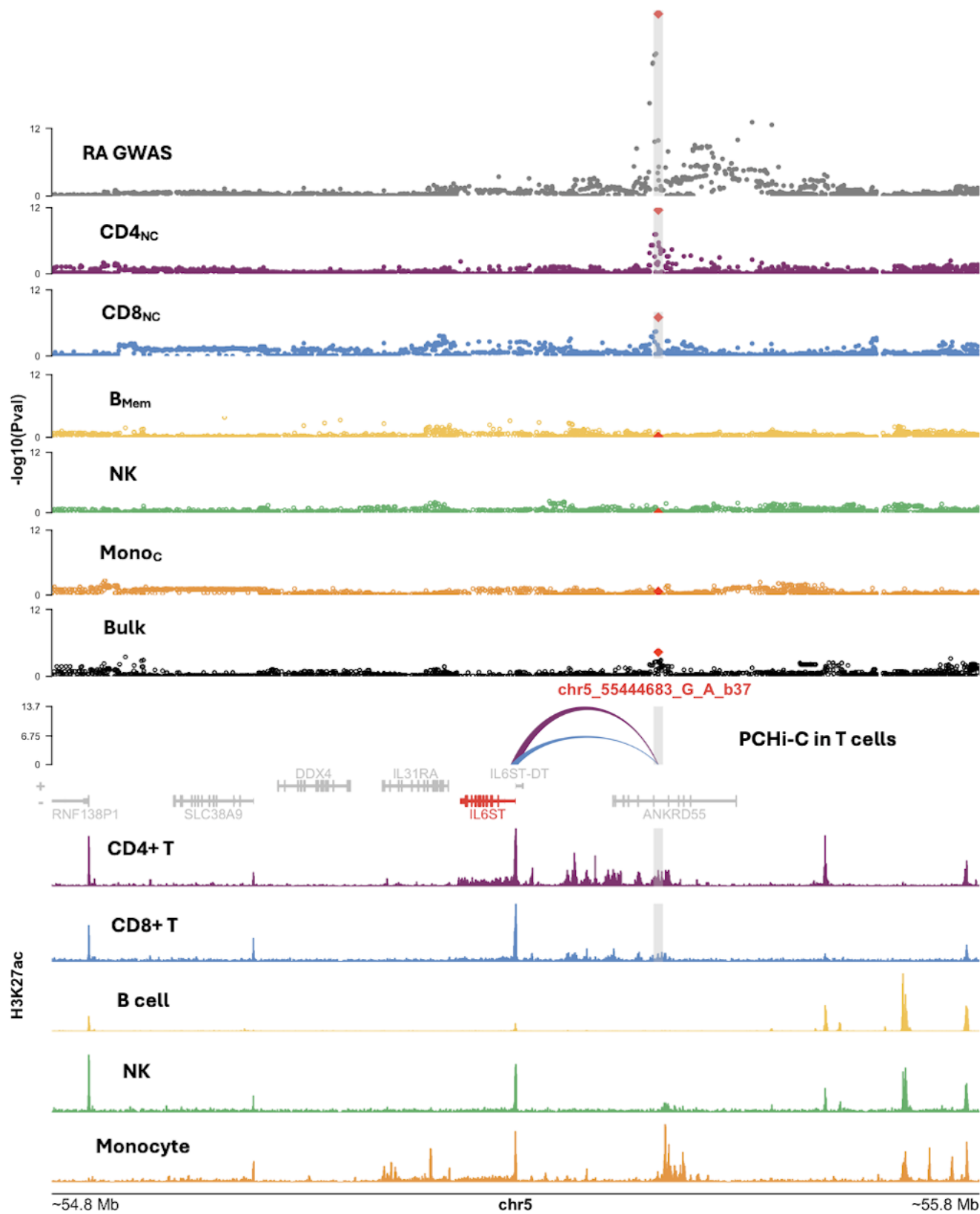
755 **(A)** We report the proportion of heritability (h^2) explained by SNP-annotations built from the union of sc-
 756 eQTLs and bulk-eQTLs for 16 GWAS blood and immune-related diseases. Error bars denote 1 standard
 757 error of the corresponding estimates. **(B)** We report S-LDSC standardized effect size (τ^*) and its
 758 associated P values obtained for 13 traits and 12 eQTL annotations; τ^* represents the proportionate
 759 change in per-SNP h^2 associated with 1 standard deviation change of annotation value after conditioning
 760 to baseline SNP-annotations. Only trait-annotation pairs with significant τ^* (after FDR correction) were
 761 plotted. The size of the dot is proportional to the standardized effect size τ^* , and the colorness of the dot
 762 is proportional to $-\log_{10}(P)$. Numerical results are reported in **Tables S16, S17**.
 763



764
 765

766 **Figure 7: sc-eQTLs prioritize candidate genes missed by bulk-eQTLs.**

767 We present an example showing that OneK1K sc-eQTLs in CD4_{NC} and CD8_{NC} can nominate *IL6ST* as a
768 candidate gene for RA, while OneK1K bulk-eQTLs cannot. We report RA GWAS results at the locus
769 highlighting GWAS leading SNP rs7731626 (chr5:55444683:G>A) (1st row), significant *IL6ST* sc-eQTLs
770 in CD4_{NC} and CD8_{NC} T cells (2nd and 3rd row), non-significant (represented by open circle) sc-eQTLs in
771 B_{Mem}, NK and Mono_C cells (4th to 6th row), non-significant bulk-eQTLs (7th row), PChi-C links ⁷³ between
772 rs7731626 loci and TSS of *IL6ST* observed in CD4+ and CD8+ T cells (height of the arch is proportional
773 to the the score of the link; 8th row), and H3K27ac peaks observed in ENCODE samples corresponding
774 to 5 cell types ^{74,75} (height of the bar is proportional to the peak intensity; 9th to 13th row). In Manhattan
775 plots, we report $-\log_{10}(P)$ of all SNPs within ± 500 kb from TSS of the *IL6ST* gene. Different colors were
776 used to represent matching cell types. The grey shade represent ± 5 kb away from rs7731626 SNP in RA
777 GWAS and plots related to T cells.



779 References

- 780 1. Giambartolomei, C., Vukcevic, D., Schadt, E.E., Franke, L., Hingorani, A.D., Wallace, C., and
781 Plagnol, V. (2014). Bayesian test for colocalisation between pairs of genetic association studies using
782 summary statistics. *PLoS Genet.* *10*, e1004383.
- 783 2. Lee, D., Williamson, V.S., Bigdeli, T.B., Riley, B.P., Fanous, A.H., Vladimirov, V.I., and Bacanu, S.-A.
784 (2015). JEPeG: a summary statistics based tool for gene-level joint testing of functional variants.
785 *Bioinformatics* *31*, 1176–1182.
- 786 3. Hormozdiari, F., van de Bunt, M., Segrè, A.V., Li, X., Joo, J.W.J., Bilow, M., Sul, J.H.,
787 Sankararaman, S., Pasaniuc, B., and Eskin, E. (2016). Colocalization of GWAS and eQTL signals
788 detects target genes. *Am. J. Hum. Genet.* *99*, 1245–1260.
- 789 4. Chun, S., Casparino, A., Patsopoulos, N.A., Croteau-Chonka, D.C., Raby, B.A., De Jager, P.L.,
790 Sunyaev, S.R., and Cotsapas, C. (2017). Limited statistical evidence for shared genetic effects of
791 eQTLs and autoimmune-disease-associated loci in three major immune-cell types. *Nat. Genet.* *49*,
792 600–605.
- 793 5. Gusev, A., Ko, A., Shi, H., Bhatia, G., Chung, W., Penninx, B.W.J.H., Jansen, R., de Geus, E.J.C.,
794 Boomsma, D.I., Wright, F.A., et al. (2016). Integrative approaches for large-scale transcriptome-wide
795 association studies. *Nat. Genet.* *48*, 245–252.
- 796 6. Gamazon, E.R., Wheeler, H.E., Shah, K.P., Mozaffari, S.V., Aquino-Michaels, K., Carroll, R.J., Eyler,
797 A.E., Denny, J.C., GTEx Consortium, Nicolae, D.L., et al. (2015). A gene-based association method for
798 mapping traits using reference transcriptome data. *Nat. Genet.* *47*, 1091–1098.
- 799 7. Mancuso, N., Shi, H., Goddard, P., Kichaev, G., Gusev, A., and Pasaniuc, B. (2017). Integrating
800 gene expression with summary association statistics to identify genes associated with 30 complex
801 traits. *Am. J. Hum. Genet.* *100*, 473–487.
- 802 8. Mancuso, N., Freund, M.K., Johnson, R., Shi, H., Kichaev, G., Gusev, A., and Pasaniuc, B. (2019).
803 Probabilistic fine-mapping of transcriptome-wide association studies. *Nat. Genet.* *51*, 675–682.
- 804 9. Wainberg, M., Sinnott-Armstrong, N., Mancuso, N., Barbeira, A.N., Knowles, D.A., Golan, D., Ermel,
805 R., Ruusalepp, A., Quertermous, T., Hao, K., et al. (2019). Opportunities and challenges for
806 transcriptome-wide association studies. *Nat. Genet.* *51*, 592–599.
- 807 10. GTEx Consortium (2020). The GTEx Consortium atlas of genetic regulatory effects across human
808 tissues. *Science* *369*, 1318–1330.
- 809 11. Vösa, U., Claringbould, A., Westra, H.-J., Bonder, M.J., Deelen, P., Zeng, B., Kirsten, H., Saha, A.,
810 Kreuzhuber, R., Yazar, S., et al. (2021). Large-scale cis- and trans-eQTL analyses identify thousands
811 of genetic loci and polygenic scores that regulate blood gene expression. *Nat. Genet.* *53*, 1300–1310.
- 812 12. Chen, L., Ge, B., Casale, F.P., Vasquez, L., Kwan, T., Garrido-Martín, D., Watt, S., Yan, Y., Kundu,
813 K., Ecker, S., et al. (2016). Genetic drivers of epigenetic and transcriptional variation in human immune
814 cells. *Cell* *167*, 1398–1414.e24.
- 815 13. Lappalainen, T., Sammeth, M., Friedländer, M.R., 't Hoen, P.A.C., Monlong, J., Rivas, M.A.,
816 González-Porta, M., Kurbatova, N., Griebel, T., Ferreira, P.G., et al. (2013). Transcriptome and genome

- 817 sequencing uncovers functional variation in humans. *Nature* 501, 506–511.
- 818 14. Taylor, D.L., Jackson, A.U., Narisu, N., Hemani, G., Erdos, M.R., Chines, P.S., Swift, A., Idol, J.,
819 Didion, J.P., Welch, R.P., et al. (2019). Integrative analysis of gene expression, DNA methylation,
820 physiological traits, and genetic variation in human skeletal muscle. *Proc. Natl. Acad. Sci. U. S. A.* 116,
821 10883–10888.
- 822 15. Mostafavi, H., Spence, J.P., Naqvi, S., and Pritchard, J.K. (2023). Systematic differences in
823 discovery of genetic effects on gene expression and complex traits. *Nat. Genet.*
- 824 16. Umans, B.D., Battle, A., and Gilad, Y. (2021). Where Are the Disease-Associated eQTLs? *Trends*
825 *Genet.* 37, 109–124.
- 826 17. Connally, N.J., Nazeen, S., Lee, D., Shi, H., Stamatoyannopoulos, J., Chun, S., Cotsapas, C.,
827 Cassa, C.A., and Sunyaev, S.R. (2022). The missing link between genetic association and regulatory
828 function. *Elife* 11,.
- 829 18. Yao, D.W., O'Connor, L.J., Price, A.L., and Gusev, A. (2020). Quantifying genetic effects on
830 disease mediated by assayed gene expression levels. *Nat. Genet.* 52, 626–633.
- 831 19. Yazar, S., Alquicira-Hernandez, J., Wing, K., Senabouth, A., Gordon, M.G., Andersen, S., Lu, Q.,
832 Rowson, A., Taylor, T.R.P., Clarke, L., et al. (2022). Single-cell eQTL mapping identifies cell type–
833 specific genetic control of autoimmune disease. *Science* 376, eabf3041.
- 834 20. Emani, P.S., Liu, J.J., Clarke, D., Jensen, M., Warrell, J., Gupta, C., Meng, R., Lee, C.Y., Xu, S.,
835 Dursun, C., et al. (2024). Single-cell genomics and regulatory networks for 388 human brains. *Science*
836 384, eadi5199.
- 837 21. The Garvan Institute of Medical Research International partnership to map 50 million human cells
838 and uncover genetic fingerprints of disease.
- 839 22. van der Wijst, M., de Vries, D.H., Groot, H.E., Trynka, G., Hon, C.C., Bonder, M.J., Stegle, O.,
840 Nawijn, M.C., Idaghdour, Y., van der Harst, P., et al. (2020). The single-cell eQTLGen consortium. *Elife*
841 9, e52155.
- 842 23. van der Wijst, M.G.P., Brugge, H., de Vries, D.H., Deelen, P., Swertz, M.A., LifeLines Cohort Study,
843 BIOS Consortium, and Franke, L. (2018). Single-cell RNA sequencing identifies celltype-specific cis-
844 eQTLs and co-expression QTLs. *Nat. Genet.* 50, 493–497.
- 845 24. de Vries, D.H., Matzaraki, V., Bakker, O.B., Brugge, H., Westra, H.-J., Netea, M.G., Franke, L.,
846 Kumar, V., and van der Wijst, M.G.P. (2020). Integrating GWAS with bulk and single-cell RNA-
847 sequencing reveals a role for LY86 in the anti-Candida host response. *PLoS Pathog.* 16, e1008408.
- 848 25. Oelen, R., de Vries, D.H., Brugge, H., Gordon, M.G., Vochteloo, M., single-cell eQTLGen
849 consortium, BIOS Consortium, Ye, C.J., Westra, H.-J., Franke, L., et al. (2022). Single-cell RNA-
850 sequencing of peripheral blood mononuclear cells reveals widespread, context-specific gene
851 expression regulation upon pathogenic exposure. *Nat. Commun.* 13, 3267.
- 852 26. van Blokland, I.V., Oelen, R., Groot, H.E., Benjamins, J.W., Pekayvaz, K., Losert, C., Knottenberg,
853 V., Heinig, M., Nicolai, L., Stark, K., et al. (2024). Single-cell dissection of the immune response after
854 acute myocardial infarction. *Circ. Genom. Precis. Med.* 17, e004374.
- 855 27. Shabalin, A.A. (2012). Matrix eQTL: ultra fast eQTL analysis via large matrix operations.

- 856 Bioinformatics 28, 1353–1358.
- 857 28. Ongen, H., Buil, A., Brown, A.A., Dermitzakis, E.T., and Delaneau, O. (2016). Fast and efficient
858 QTL mapper for thousands of molecular phenotypes. *Bioinformatics* 32, 1479–1485.
- 859 29. Taylor-Weiner, A., Aguet, F., Haradhvala, N.J., Gosai, S., Anand, S., Kim, J., Ardlie, K., Van Allen,
860 E.M., and Getz, G. (2019). Scaling computational genomics to millions of individuals with GPUs.
861 *Genome Biol.* 20, 228.
- 862 30. Hafemeister, C., and Satija, R. (2019). Normalization and variance stabilization of single-cell RNA-
863 seq data using regularized negative binomial regression. *Genome Biol.* 20, 296.
- 864 31. Ahlmann-Eltze, C., and Huber, W. (2023). Comparison of transformations for single-cell RNA-seq
865 data. *Nat. Methods* 1–8.
- 866 32. Warton, D.I. (2018). Why you cannot transform your way out of trouble for small counts. *Biometrics*
867 74, 362–368.
- 868 33. Beasley, T.M., Erickson, S., and Allison, D.B. (2009). Rank-based inverse normal transformations
869 are increasingly used, but are they merited? *Behav. Genet.* 39, 580–595.
- 870 34. Nathan, A., Asgari, S., Ishigaki, K., Valencia, C., Amariuta, T., Luo, Y., Beynor, J.I., Baglaenko, Y.,
871 Suliman, S., Price, A.L., et al. (2022). Single-cell eQTL models reveal dynamic T cell state dependence
872 of disease loci. *Nature* 606, 120–128.
- 873 35. Cuomo, A.S.E., Heinen, T., Vagiaki, D., Horta, D., Marioni, J.C., and Stegle, O. (2022).
874 CellRegMap: a statistical framework for mapping context-specific regulatory variants using scRNA-seq.
875 *Mol. Syst. Biol.* 18, e10663.
- 876 36. Zhou, W., Cuomo, A.S.E., Xue, A., Kanai, M., Chau, G., Krishna, C., Xavier, R.J., MacArthur, D.G.,
877 Powell, J.E., Daly, M.J., et al. (2024). Efficient and accurate mixed model association tool for single-cell
878 eQTL analysis. *medRxiv* 2024.05.15.24307317.
- 879 37. Mu, Z., Wei, W., Fair, B., Miao, J., Zhu, P., and Li, Y.I. (2021). The impact of cell type and context-
880 dependent regulatory variants on human immune traits. *Genome Biol.* 22, 122.
- 881 38. Radhakrishna Rao, C. (1948). Large sample tests of statistical hypotheses concerning several
882 parameters with applications to problems of estimation. *Math. Proc. Camb. Philos. Soc.* 44, 50–57.
- 883 39. Liu, Y., Chen, S., Li, Z., Morrison, A.C., Boerwinkle, E., and Lin, X. (2019). ACAT: A fast and
884 powerful p value combination method for rare-variant analysis in sequencing studies. *Am. J. Hum.*
885 *Genet.* 104, 410–421.
- 886 40. Ouwens, K.G., Jansen, R., Nivard, M.G., van Dongen, J., Frieser, M.J., Hottenga, J.-J., Arindrarto,
887 W., Claringbould, A., van Ijzerman, M., Mei, H., et al. (2020). A characterization of cis- and trans-
888 heritability of RNA-Seq-based gene expression. *Eur. J. Hum. Genet.* 28, 253–263.
- 889 41. Ahlmann-Eltze, C., and Huber, W. (2021). glmGamPoi: fitting Gamma-Poisson generalized linear
890 models on single cell count data. *Bioinformatics* 36, 5701–5702.
- 891 42. Grün, D., Kester, L., and van Oudenaarden, A. (2014). Validation of noise models for single-cell
892 transcriptomics. *Nat. Methods* 11, 637–640.

- 893 43. Svensson, V. (2020). Droplet scRNA-seq is not zero-inflated. *Nat. Biotechnol.* 38, 147–150.
- 894 44. McCarthy, D.J., Chen, Y., and Smyth, G.K. (2012). Differential expression analysis of multifactor
895 RNA-Seq experiments with respect to biological variation. *Nucleic Acids Res.* 40, 4288–4297.
- 896 45. Robinson, M.D., McCarthy, D.J., and Smyth, G.K. (2010). edgeR: a Bioconductor package for
897 differential expression analysis of digital gene expression data. *Bioinformatics* 26, 139–140.
- 898 46. Love, M.I., Huber, W., and Anders, S. (2014). Moderated estimation of fold change and dispersion
899 for RNA-seq data with DESeq2. *Genome Biol.* 15, 550.
- 900 47. Perez, R.K., Gordon, M.G., Subramaniam, M., Kim, M.C., Hartoularos, G.C., Targ, S., Sun, Y.,
901 Ogorodnikov, A., Bueno, R., Lu, A., et al. (2022). Single-cell RNA-seq reveals cell type-specific
902 molecular and genetic associations to lupus. *Science* 376, eabf1970.
- 903 48. Schmiedel, B.J., Singh, D., Madrigal, A., Valdovino-Gonzalez, A.G., White, B.M., Zapardiel-
904 Gonzalo, J., Ha, B., Altay, G., Greenbaum, J.A., McVicker, G., et al. (2018). Impact of genetic
905 polymorphisms on human immune cell gene expression. *Cell* 175, 1701–1715.e16.
- 906 49. Lu, Z., Wang, X., Carr, M., Kim, A., Gazal, S., Mohammadi, P., Wu, L., Gusev, A., Pirruccello, J.,
907 Kachuri, L., et al. (2024). Improved multi-ancestry fine-mapping identifies cis-regulatory variants
908 underlying molecular traits and disease risk. *medRxiv* 2024.04.15.24305836.
- 909 50. Wang, X., and Goldstein, D.B. (2020). Enhancer Domains Predict Gene Pathogenicity and Inform
910 Gene Discovery in Complex Disease. *Am. J. Hum. Genet.* 106, 215–233.
- 911 51. Glassberg, E.C., Gao, Z., Harpak, A., Lan, X., and Pritchard, J.K. (2019). Evidence for weak
912 selective constraint on human gene expression. *Genetics* 211, 757–772.
- 913 52. Mohammadi, P., Castel, S.E., Brown, A.A., and Lappalainen, T. (2017). Quantifying the regulatory
914 effect size of cis-acting genetic variation using allelic fold change. *Genome Res.* 27, 1872–1884.
- 915 53. Taylor, D.J., Chhetri, S.B., Tassia, M.G., Biddanda, A., Yan, S.M., Wojcik, G.L., Battle, A., and
916 McCoy, R.C. (2024). Sources of gene expression variation in a globally diverse human cohort. *Nature*
917 632, 122–130.
- 918 54. Zou, Y., Carbonetto, P., Wang, G., and Stephens, M. (2022). Fine-mapping from summary data
919 with the “Sum of Single Effects” model. *PLoS Genet.* 18, e1010299.
- 920 55. Finucane, H.K., Bulik-Sullivan, B., Gusev, A., Trynka, G., Reshef, Y., Loh, P.-R., Anttila, V., Xu, H.,
921 Zang, C., Farh, K., et al. (2015). Partitioning heritability by functional annotation using genome-wide
922 association summary statistics. *Nat. Genet.* 47, 1228–1235.
- 923 56. Liu, X., Finucane, H.K., Gusev, A., Bhatia, G., Gazal, S., O’Connor, L., Bulik-Sullivan, B., Wright,
924 F.A., Sullivan, P.F., Neale, B.M., et al. (2017). Functional Architectures of Local and Distal Regulation
925 of Gene Expression in Multiple Human Tissues. *Am. J. Hum. Genet.* 100, 605–616.
- 926 57. Sakaue, S., Weinand, K., Isaac, S., Dey, K.K., Jagadeesh, K., Kanai, M., Watts, G.F.M., Zhu, Z.,
927 Accelerating Medicines Partnership® RA/SLE Program and Network, Brenner, M.B., et al. (2024).
928 Tissue-specific enhancer-gene maps from multimodal single-cell data identify causal disease alleles.
929 *Nat. Genet.* 56, 615–626.
- 930 58. Uribut, S.M., Wang, G., Carbonetto, P., and Stephens, M. (2019). Flexible statistical methods for

- 931 estimating and testing effects in genomic studies with multiple conditions. *Nat. Genet.* *51*, 187–195.
- 932 59. Chen, M., and Dahl, A. (2024). A robust model for cell type-specific interindividual variation in
933 single-cell RNA sequencing data. *Nat. Commun.* *15*, 5229.
- 934 60. Heinz, S., Romanoski, C.E., Benner, C., and Glass, C.K. (2015). The selection and function of cell
935 type-specific enhancers. *Nat. Rev. Mol. Cell Biol.* *16*, 144–154.
- 936 61. Jin, F., Li, Y., Dixon, J.R., Selvaraj, S., Ye, Z., Lee, A.Y., Yen, C.-A., Schmitt, A.D., Espinoza, C.A.,
937 and Ren, B. (2013). A high-resolution map of the three-dimensional chromatin interactome in human
938 cells. *Nature* *503*, 290–294.
- 939 62. Rosenberg, J., and Huang, J. (2018). CD8+ T cells and NK cells: Parallel and complementary
940 soldiers of immunotherapy. *Curr. Opin. Chem. Eng.* *19*, 9–20.
- 941 63. Trynka, G., Sandor, C., Han, B., Xu, H., Stranger, B.E., Liu, X.S., and Raychaudhuri, S. (2013).
942 Chromatin marks identify critical cell types for fine mapping complex trait variants. *Nat. Genet.* *45*, 124–
943 130.
- 944 64. Kim, A., Zhang, Z., Legros, C., Lu, Z., de Smith, A., Moore, J.E., Mancuso, N., and Gazal, S.
945 (2024). Inferring causal cell types of human diseases and risk variants from candidate regulatory
946 elements. medRxiv.
- 947 65. Finucane, H.K., Reshef, Y.A., Anttila, V., Slowikowski, K., Gusev, A., Byrnes, A., Gazal, S., Loh, P.-
948 R., Lareau, C., Shores, N., et al. (2018). Heritability enrichment of specifically expressed genes
949 identifies disease-relevant tissues and cell types. *Nat. Genet.* *50*, 621–629.
- 950 66. Jagadeesh, K.A., Dey, K.K., Montoro, D.T., Mohan, R., Gazal, S., Engreitz, J.M., Xavier, R.J., Price,
951 A.L., and Regev, A. (2022). Identifying disease-critical cell types and cellular processes by integrating
952 single-cell RNA-sequencing and human genetics. *Nat. Genet.* *54*, 1479–1492.
- 953 67. Zhang, M.J., Hou, K., Dey, K.K., Sakaue, S., Jagadeesh, K.A., Weinand, K., Taychameekiatchai,
954 A., Rao, P., Pisco, A.O., Zou, J., et al. (2022). Polygenic enrichment distinguishes disease associations
955 of individual cells in single-cell RNA-seq data. *Nat. Genet.* *54*, 1572–1580.
- 956 68. Müller-Ladner, U., Pap, T., Gay, R.E., Neidhart, M., and Gay, S. (2005). Mechanisms of disease:
957 the molecular and cellular basis of joint destruction in rheumatoid arthritis. *Nat. Clin. Pract. Rheumatol.*
958 *1*, 102–110.
- 959 69. Mack, M.R., Brestoff, J.R., Berrien-Elliott, M.M., Trier, A.M., Yang, T.-L.B., McCullen, M., Collins,
960 P.L., Niu, H., Bodet, N.D., Wagner, J.A., et al. (2020). Blood natural killer cell deficiency reveals an
961 immunotherapy strategy for atopic dermatitis. *Sci. Transl. Med.* *12*, eaay1005.
- 962 70. Ishigaki, K., Sakaue, S., Terao, C., Luo, Y., Sonehara, K., Yamaguchi, K., Amariuta, T., Too, C.L.,
963 Laufer, V.A., Scott, I.C., et al. (2022). Multi-ancestry genome-wide association analyses identify novel
964 genetic mechanisms in rheumatoid arthritis. *Nat. Genet.* *54*, 1640–1651.
- 965 71. Okada, Y., Wu, D., Trynka, G., Raj, T., Terao, C., Ikari, K., Kochi, Y., Ohmura, K., Suzuki, A.,
966 Yoshida, S., et al. (2014). Genetics of rheumatoid arthritis contributes to biology and drug discovery.
967 *Nature* *506*, 376–381.
- 968 72. Westra, H.-J., Martínez-Bonet, M., Onengut-Gumuscu, S., Lee, A., Luo, Y., Teslovich, N.,
969 Worthington, J., Martin, J., Huizinga, T., Klareskog, L., et al. (2018). Fine-mapping and functional

- 970 studies highlight potential causal variants for rheumatoid arthritis and type 1 diabetes. *Nat. Genet.* *50*,
971 1366–1374.
- 972 73. Javierre, B.M., Burren, O.S., Wilder, S.P., Kreuzhuber, R., Hill, S.M., Sewitz, S., Cairns, J., Wingett,
973 S.W., Várnai, C., Thiecke, M.J., et al. (2016). Lineage-Specific Genome Architecture Links Enhancers
974 and Non-coding Disease Variants to Target Gene Promoters. *Cell* *167*, 1369–1384.e19.
- 975 74. ENCODE Project Consortium (2012). An integrated encyclopedia of DNA elements in the human
976 genome. *Nature* *489*, 57–74.
- 977 75. Luo, Y., Hitz, B.C., Gabdank, I., Hilton, J.A., Kagda, M.S., Lam, B., Myers, Z., Sud, P., Jou, J., Lin,
978 K., et al. (2020). New developments on the Encyclopedia of DNA Elements (ENCODE) data portal.
979 *Nucleic Acids Res.* *48*, D882–D889.
- 980 76. Mena, J., Alloza, I., Tulloch Navarro, R., Aldekoa, A., Díez García, J., Villanueva Etxebarria, A.,
981 Lindskog, C., Antigüedad, A., Boyero, S., Mendibe-Bilbao, M.D.M., et al. (2021). Genomic multiple
982 sclerosis risk variants modulate the expression of the ANKRD55-IL6ST gene region in immature
983 dendritic cells. *Front. Immunol.* *12*, 816930.
- 984 77. Lessard, S., Chao, M., Reis, K., Beauvais, M., Rajpal, D.K., Shankara, S., Sloane, J., Palta, P.,
985 Klinger, K., de Rinaldis, E., et al. (2023). Leveraging large-scale multi-omics to identify therapeutic
986 targets from genome-wide association studies.
- 987 78. Benaglio, P., Newsome, J., Han, J.Y., Chiou, J., Aylward, A., Corban, S., Miller, M., Okino, M.-L.,
988 Kaur, J., Preissl, S., et al. (2023). Mapping genetic effects on cell type-specific chromatin accessibility
989 and annotating complex immune trait variants using single nucleus ATAC-seq in peripheral blood.
990 *PLoS Genet.* *19*, e1010759.
- 991 79. Jang, S., Kwon, E.-J., and Lee, J.J. (2022). Rheumatoid arthritis: Pathogenic roles of diverse
992 immune cells. *Int. J. Mol. Sci.* *23*, 905.
- 993 80. Pearce, E.L., Mullen, A.C., Martins, G.A., Krawczyk, C.M., Hutchins, A.S., Zediak, V.P., Banica, M.,
994 DiCioccio, C.B., Gross, D.A., Mao, C.-A., et al. (2003). Control of effector CD8+ T cell function by the
995 transcription factor Eomesodermin. *Science* *302*, 1041–1043.
- 996 81. Elgueta, R., Benson, M.J., de Vries, V.C., Wasiuk, A., Guo, Y., and Noelle, R.J. (2009). Molecular
997 mechanism and function of CD40/CD40L engagement in the immune system. *Immunol. Rev.* *229*, 152–
998 172.
- 999 82. Li, G., Diogo, D., Wu, D., Spoonamore, J., Dancik, V., Franke, L., Kurreeman, F., Rossin, E.J.,
1000 Duclos, G., Hartland, C., et al. (2013). Human genetics in rheumatoid arthritis guides a high-throughput
1001 drug screen of the CD40 signaling pathway. *PLoS Genet.* *9*, e1003487.
- 1002 83. Rose-John, S. (2018). Interleukin-6 family cytokines. *Cold Spring Harb. Perspect. Biol.* *10*,
1003 a028415.
- 1004 84. Ernst, M., and Jenkins, B.J. (2004). Acquiring signalling specificity from the cytokine receptor
1005 gp130. *Trends Genet.* *20*, 23–32.
- 1006 85. Rose-John, S., Jenkins, B.J., Garbers, C., Moll, J.M., and Scheller, J. (2023). Targeting IL-6 trans-
1007 signalling: past, present and future prospects. *Nat. Rev. Immunol.* *23*, 666–681.
- 1008 86. Weeks, E.M., Ulirsch, J.C., Cheng, N.Y., Trippe, B.L., Fine, R.S., Miao, J., Patwardhan, T.A., Kanai,

- 1009 M., Nasser, J., Fulco, C.P., et al. (2023). Leveraging polygenic enrichments of gene features to predict
1010 genes underlying complex traits and diseases. *Nat. Genet.* 1–10.
- 1011 87. Mu, Z., Randolph, H.E., Aguirre-Gamboa, R., Ketter, E., Dumaine, A., Locher, V., Brandolino, C.,
1012 Liu, X., Kaufmann, D.E., Barreiro, L.B., et al. (2024). Impact of disease-associated chromatin
1013 accessibility QTLs across immune cell types and contexts.
- 1014 88. Gutierrez-Arcelus, M., Baglaenko, Y., Arora, J., Hannes, S., Luo, Y., Amariuta, T., Teslovich, N.,
1015 Rao, D.A., Ermann, J., Jonsson, A.H., et al. (2020). Allele-specific expression changes dynamically
1016 during T cell activation in HLA and other autoimmune loci. *Nat. Genet.* 52, 247–253.
- 1017 89. The Developmental Genotype-Tissue Expression (dGTE_x) project.
- 1018 90. Tian, C., Zhang, Y., Tong, Y., Kock, K.H., Sim, D.Y., Liu, F., Dong, J., Jing, Z., Wang, W., Gao, J.,
1019 et al. (2024). Single-cell RNA sequencing of peripheral blood links cell-type-specific regulation of
1020 splicing to autoimmune and inflammatory diseases. *Nat. Genet.* 56, 2739–2752.
- 1021 91. Hormozdiari, F., Gazal, S., van de Geijn, B., Finucane, H.K., Ju, C.J.-T., Loh, P.-R., Schoech, A.,
1022 Reshef, Y., Liu, X., O'Connor, L., et al. (2018). Leveraging molecular quantitative trait loci to understand
1023 the genetic architecture of diseases and complex traits. *Nat. Genet.* 50, 1041–1047.
- 1024 92. Wang, J., Zhang, Z., Lu, Z., Mancuso, N., and Gazal, S. (2024). Genes with differential expression
1025 across ancestries are enriched in ancestry-specific disease effects likely due to gene-by-environment
1026 interactions. *Am. J. Hum. Genet.*
- 1027 93. Hilbe, J.M. (2011). Negative binomial regression. In *Negative Binomial Regression*, (Cambridge:
1028 Cambridge University Press), pp. 185–220.
- 1029 94. Engle, R.F. (1984). Chapter 13 Wald, likelihood ratio, and Lagrange multiplier tests in econometrics.
1030 In *Handbook of Econometrics*, (Elsevier), pp. 775–826.
- 1031 95. Lin, W., Schmidt, M., and Khan, M.E. (2020). Handling the Positive-Definite Constraint in the
1032 Bayesian Learning Rule.
- 1033 96. Storey, J.D., Bass, A.J., Dabney, A., and Robinson, D. (2015). *qvalue: Q-value estimation for false*
1034 *discovery rate control. R Package Version 2*, 10–18129.
- 1035 97. McCaw, Z.R., Lane, J.M., Saxena, R., Redline, S., and Lin, X. (2020). Operating characteristics of
1036 the rank-based inverse normal transformation for quantitative trait analysis in genome-wide association
1037 studies. *Biometrics* 76, 1262–1272.
- 1038 98. Kerimov, N., Hayhurst, J.D., Peikova, K., Manning, J.R., Walter, P., Kolberg, L., Samoviča, M.,
1039 Sakthivel, M.P., Kuzmin, I., Trevanion, S.J., et al. (2021). A compendium of uniformly processed human
1040 gene expression and splicing quantitative trait loci. *Nat. Genet.* 53, 1290–1299.
- 1041 99. Stefansson, H., Helgason, A., Thorleifsson, G., Steinthorsdottir, V., Masson, G., Barnard, J., Baker,
1042 A., Jonasdottir, A., Ingason, A., Gudnadottir, V.G., et al. (2005). A common inversion under selection in
1043 Europeans. *Nat. Genet.* 37, 129–137.
- 1044 100. Zody, M.C., Jiang, Z., Fung, H.-C., Antonacci, F., Hillier, L.W., Cardone, M.F., Graves, T.A., Kidd,
1045 J.M., Cheng, Z., Abouelleil, A., et al. (2008). Evolutionary toggling of the MAPT 17q21.31 inversion
1046 region. *Nat. Genet.* 40, 1076–1083.

- 1047 101. Chiou, J., Geusz, R.J., Okino, M.-L., Han, J.Y., Miller, M., Melton, R., Beebe, E., Benaglio, P.,
1048 Huang, S., Korgaonkar, K., et al. (2021). Interpreting type 1 diabetes risk with genetics and single-cell
1049 epigenomics. *Nature* 594, 398–402.
- 1050 102. Wen, X. (2016). Molecular QTL discovery incorporating genomic annotations using Bayesian false
1051 discovery rate control. *Aoas* 10, 1619–1638.
- 1052 103. Gazal, S., Marquez-Luna, C., Finucane, H.K., and Price, A.L. (2019). Reconciling S-LDSC and
1053 LDK functional enrichment estimates. *Nat. Genet.* 51, 1202–1204.
- 1054 104. van de Geijn, B., Finucane, H., Gazal, S., Hormozdiari, F., Amariuta, T., Liu, X., Gusev, A., Loh,
1055 P.-R., Reshef, Y., Kichaev, G., et al. (2020). Annotations capturing cell type-specific TF binding explain
1056 a large fraction of disease heritability. *Hum. Mol. Genet.* 29, 1057–1067.
- 1057